Final Technical Report

Simulation and Modeling of Wood Dust Combustion in Cyclone Burners

Prepared by:
Stephen M. de Bruyn Kops and Philip C. Malte
Energy and Environmental Combustion Laboratory
Department of Mechanical Engineering
University of Washington

Prepared for:
U. S. Department of Energy

January 30, 2004

Abstract

The wood products industry generates substantial amounts of saw and sander dust as part of normal operations. To dispose of this waste and to generate heat for industrial processes, the dust is burned, which can produce significant pollutant emissions, such as oxides of nitrogen (NOx). A step in reducing emissions from wood dust combustion is to identify under what conditions in the commercial dust burners the pollutants are being formed. As research in this area, the operating characteristics of a typical dust burner are examined by numerically simulating the device in three-dimensions using a commercial computational fluid dynamics (CFD) package. The hydrodynamic characteristics of the flow are examined, as are the major species and temperature fields. Especially, the production of NOx is examined.

The NOx model being used requires, among other parameters, inputs for the fraction of fuel nitrogen that devolatalizes and the surface area of the char particles responsible for the reduction of NO to N_2 (BET surface area), and neither of these quantities is well known for wood dust. Decreasing the BET surface area has the same effect as decreasing the volatile nitrogen fraction, i.e., it increases the exit plane NOx concentration. Fortunately, the concentration of NOx at the exit plane increases by only a factor of 1.9 when the BET surface area is reduced from 25000 to 0 (m2=kg) and the volatile nitrogen fraction is reduced from 93% to 50%. The conclusion is that modest uncertainty in either of the input parameters will not lead to significant errors in the NOx predictions. This encourages the thought that the simulations can lead to insight into how to reduce NOx emissions from wood dust burners.

Contents

1 Introduction 1

2 Physical Problem and Models 2
2.1 Hydrodynamics 2
2.2 Particle Tracking 4
2.3 Fuel Devolatilization and Char Combustion 6
2.3.1 Devolatilization Submodel 7
2.3.2 Surface Reaction Submodel 7
2.4 Gas-phase Mixing and Reaction 9
2.4.1 Reduced Finite Rate Mechanism 11
2.5 NOx Production 12
2.5.1 Thermal NOx 13
2.5.2 Fuel NOx 15
2.5.3 The E_ects of Turbulent Fluctuations 20

3 Numerical Simulations 22
3.1 Hydrodynamic Validation 23
3.2 Temperatures and Species Concentrations 26

4 NOx Production 33

5 Conclusions 42

List of Figures

2.1 Manufacturer's drawing of the burner 3
2.2 Model geometry used in the simulations 3
2.3 Sample of the numerical grid 5
2.4 Devolatilization rate (left panel) and fraction of the particle mass not devolatilized versus time for various temperatures (right panel) 8
2.5 Behavior of the kinetic/diffusion surface reaction model for two particle sizes. 10
2.6 Pathways for the production of fuel-NOx 16

3.1 Velocity magnitude (m/s) at the midplane. The top panel is with RSM modeling, the bottom with KE modeling 24
3.2 Total pressure on the vertical centerline plane with fuel entering from the top. 25
3.3 Static temperature (K) on the vertical, centerline plane with fuel entering from the top. 29
3.4 Mass fraction O_2 on the vertical, centerline plane with fuel entering from the top. 30
3.5 Mass fraction CO_2 on the vertical, centerline plane. 31
3.6 Mass fraction CO on the vertical, centerline plane for simulation W2. 32

4.1 Mass fraction NO and HCN on the vertical, centerline plane for simulation W2-1. 37
4.2 Mass fraction NO and HCN on the vertical, centerline plane for simulation W2-2. 38
4.3 Mass fraction NO and HCN on the vertical, centerline plane for simulation W2-3. 39
4.4 Mass fraction NO and HCN on the vertical, centerline plane for simulation W2-4. 40
4.5 Mass fraction NO and HCN on the vertical, centerline plane for simulation W2-5. 41

List of Tables

2.1 Parameters affecting the surface reaction rate submodel. 9

3.1 Summary of the simulations. 22
3.2 Summary of hydrodynamic data. 23
3.3 Summary of temperatures and species concentrations. 27

4.1 NOx mass fractions and concentrations at the exit plane of simulation W2. 34

Chapter 1

Introduction

Substantial quantities of saw and sander dust produced by the wood products industry are burned to produce heat for wood drying and other applications, and the combustion process can lead to the generation of significant concentrations of pollutants. Of particular concern is the emission of oxides of nitrogen (NO_x), which are precursors to photochemical smog. A cost-effective method of reducing NO_x generation is to alter the flow field in the combustion chamber. Unfortunately, the conditions inside an industrial burner are unknown and are currently difficult or impossible to measure. An alternative to collecting data directly from the physical burner is to simulate the device numerically. The simulation of a commercial, cyclonic suspension, wood dust burner is the focus of the current research.

A review of the archived literature reveals no research involving simulations of cyclonic suspension wood dust burners, but significant advances have been made in simulating both confined vortices and the combustion of coal in vortex combustors. Hogg and Leschziner (1989a,b) report simulations of a confined swirling flow with and without density stratification and demonstrate the characteristics of several turbulence models. Chen and Lin (1999) show that a quadratic pressure-strain model is required for accurate predictions of certain highly swirling flows. Boysan et al. (1986) and Zhang and Nieh (1997) report on modeling and simulating coal-fired cyclone combustors.

The particular burner examined is the McConnell Model 48. In this report, the modeling assumptions applied to the burner and to the wood combustion process are discussed, and the velocity, temperature, and scalar fields for the major species are presented. Also reported are the operating characteristics of the burner when the fuel is methane, since this is an easier problem to solve numerically and, therefore, simplifies the evaluation of the models used for the fluid dynamics.

Chapter 2

Physical Problem and Models

Reducing a complex physical problem to a series of models that can be solved numerically requires that a number of assumptions be made. In particular, (1) for most engineering problems, the species and momentum transport equations must be modeled so that they can be solved with available computers, (2) the hydrodynamic boundary conditions must be simplified so as to adequately describe the problem without being overly complex, and (3) the combustion process must be reduced to a series of models that capture the physical phenomena involved while being practical to solve. In this section, the hydrodynamic models are considered first, followed by discussions of the models used for studying wood particle combustion, including the reduced chemical kinetic mechanisms employed and the assumptions involved in predicting the production of oxides of nitrogen (NO_x).

2.1 Hydrodynamics

The Model 48 combustor is a cyclonic suspension burner with a nominal firing rate of 40 MMBtu/hr (11,700 kW) higher heating value basis and an air flow rate into the primary combustion chamber of 13,910 scfm (at 70°F). The primary combustion chamber is a refractory-lined drum with an inside diameter of 48 inches (1.22 meters) and a length of 100 inches (2.54 meters). Combustion gases leave the primary chamber through an orifice, termed "the choke," having an inside diameter of about 18 inches (0.59 meters). A sketch of the burner is given in Fig. 2.1 and the model geometry used in the simulation in Fig. 2.2.

Air enters the combustion chamber through 14 tuyéres located along the length of the drum, seven on each side. Air also serves to transport the wood dust into the burner, and a small amount

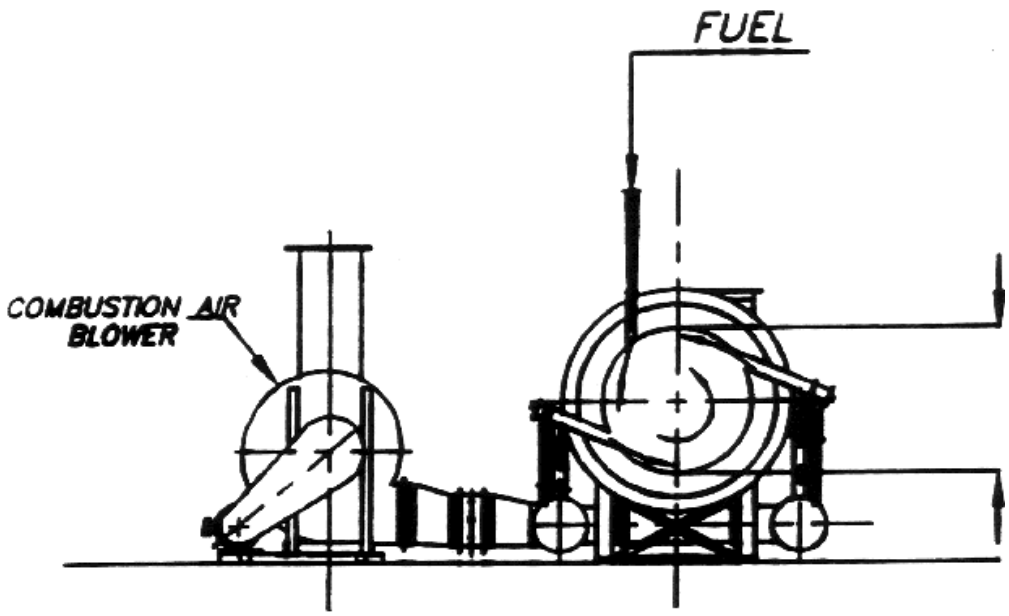

Figure 2.1: Manufacturer's drawing of the cyclonic wood dust burner primary chamber of the type used in the McConnell Model 48 burner. The dimension between the arrows at the right is 48 inches.

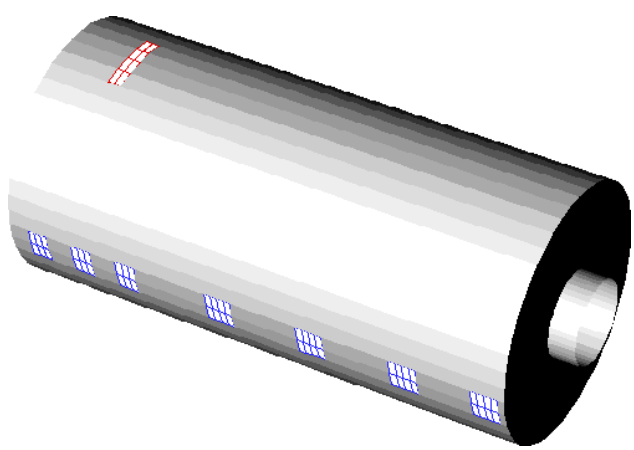

Figure 2.2: Model geometry used in the simulations of the McConnell Model 48 burner. The inlet at the top is for fuel. The side inlet are the air tuyéres.

of air enters at the center of the front-end dome to cool that surface. In the model, the inlet boundary conditions for each tuyére specify that a mass flow rate proportional to the area of that tuyére enters the combustion chamber with a direction such that the radial, tangential, and axial components of the velocity vector are proportional to (0.52, 0.85, 0). For the outlet boundary condition, a radial equilibrium pressure distribution is assumed so that the pressure at the outlet satisfies

$$\frac{\partial p}{r} = \frac{\rho v_\theta^2}{r} \ , \qquad p(r=0) = p_0 \ , \tag{2.1}$$

where r is the radial distance from the centerline, v_θ is the tangential component of the velocity, and p_0 is the pressure on centerline taken to be one atmosphere (101.3 kPa). Inherent in this boundary condition is the assumption that the radial component of the velocity is zero. The wall is considered to be adiabatic, and the standard log law of the wall (Launder and Spalding, 1974) is assumed in the computation of the mean velocity.

The simulations are computed using the commercial CFD program FLUENT, which solves the Reynolds averaged Navier-Stokes equations using a low order finite volume scheme. In this work, the steady-state solution is computed using second-order discretization for all equations. The momentum equations are closed using one of three methods: standard k-ϵ model, renormalized group k-ϵ (RNG), and seven-equation Reynolds stress model (RSM). The species transport equations and the energy equation are closed by assuming a turbulent Schmidt number of 0.7 and a turbulent Prandtl number of 0.85.

The numerical grid was constructed as a structured mesh with hexahedral elements arrayed along spokes. It was then adapted locally to reduce the maximum change in temperature and turbulence kinetic energy across a grid volume to 3 K and 30 m^2/s^2, respectively. Even with the adapted grid, there are greater than 2000 wall units between the wall and the first grid point, where a wall unit is defined as $y^+ \equiv \rho u_\tau y/\mu$, $u_\tau \equiv \sqrt{\tau_w/\rho_w}$ is the friction velocity, ρ is the density, y is the location of the first grid point, and the subscript w indicates that the quantity is evaluated at the wall. A sample of the numerical grid is shown as Fig. 2.3.

2.2 Particle Tracking

In FLUENT, the solution of the gas phase equations is only loosely coupled with the solution of the particle trajectories. Once an initial fluid flow solution is computed, the trajectories of the fuel

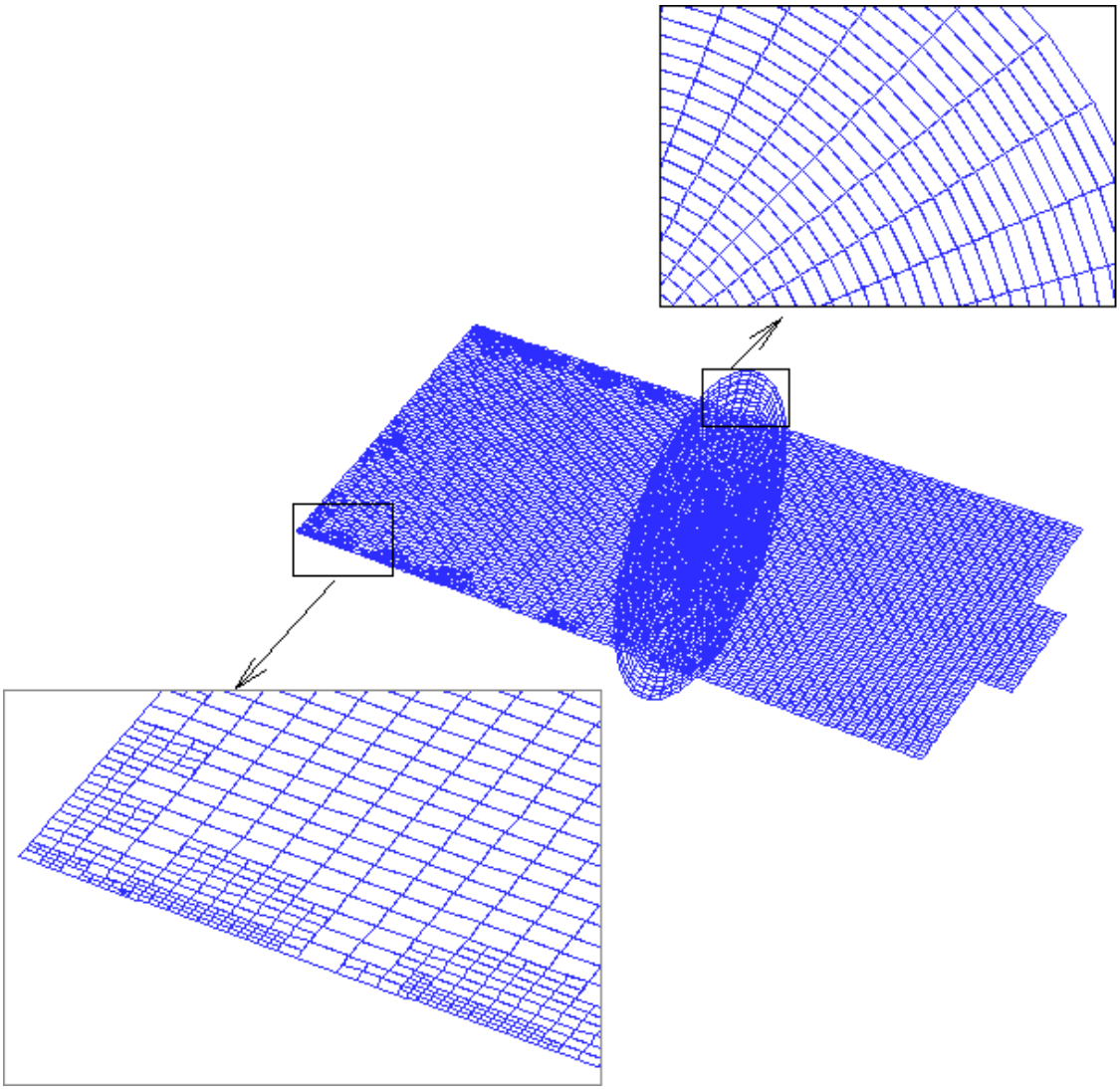

Figure 2.3: Sample of the numerical grid.

particles are determined by integrating the force balance on the particles in a Lagrangian reference frame. As this integration proceeds, source terms for species, momentum, and energy are recorded for use in the gas phase equations. Upon completion of the Lagrangian tracking procedure, solution of the gas phase solution is resumed. Iteration between the gas phase and particle tracking solutions is repeated until a converged solution is reached.

It is impractical to track all the particles that enter the burner at a particular time. Instead, the trajectories of a relatively small number of particle packets are computed and considered to be representative of all of the particles. Malte et al. (1996) report the size distribution of wood particles in a typical dust sample in 12 increments from 25 to 575 μm. In the simulations, a particle packet representing particles in each increment is introduced at four locations on the fuel inlet for a total of 48 particle packets. A stochastic process is then applied to each packet trajectory to model the effects of turbulence with the result that 4800 packets are ultimately tracked. The Lagrangian solution procedure is carried out for each packet as if it consisted of a single particle of the specified size, but the species, momentum, and energy source terms incorporated into the gas phase equations are scaled to account for the fact the the packet represents many particles.

2.3 Fuel Devolatilization and Char Combustion

The combustion of solid particles is a complex process involving heat transfer, fluid dynamics, and chemical kinetics (Smoot and Smith, 1985; Tillman, 1991). A general model that is used for many solid fuels consists of three stages of combustion (Tillman, 1991):

1. fuel heating and drying
2. particle pyrolysis to produce volatiles and carbonaceous char
3. char oxidation and volatile combustion in the gas phase

The second stage can be decomposed into several steps whereby some of the volatiles devolve directly from the solid while others pass through an intermediate tar stage. Malte et al. (1996) analyze the rate at which volatiles are formed within this framework. In the current simulations, we assume that the wood devolatilizes to the gaseous phase directly. Therefore, four combustion submodels are invoked: (1) devolatilization, (2) heterogenous char combustion, (3) gas phase mixing, and (4) gas phase reactions.

2.3.1 Devolatilization Submodel

There are several approaches to defining the rate at which volatiles enter the gas phase. The simplest is to assume that devolatilization occurs at a constant rate. Badzioch and Hawksley (1970) proposed a more realistic first-order reaction rate proportional to the amount of volatiles remaining in the particle. This model is problematic when applied to coal combustion because of the need to relate the mass of volatiles measured by proximate analysis to the mass of volatiles that will occur under particular combustion conditions (Smoot and Smith, 1985), and so more sophisticated models were developed for that application (Anthony and Howard, 1975; Kobayashi et al., 1976). Limited data are available, however, for wood devolatilization which makes the application of advanced models impractical; in this work, the first-order reaction model is assumed.

The first-order reaction model can be written

$$\frac{dm_p(t)}{dt} = -k_v[m_p(t) - m_{p0}(1 - f_{v0})] \ , \tag{2.2}$$

where $k_v = A\exp(-E/RT)$ is a kinetic rate constant, $m_p(t)$ is the mass of the particle as a function of time, $m_{p_0} = m_p(t = 0)$, and f_{v0} is the initial volatile fraction of the particle. Using data from Nunn et al. (1985), Malte et al. (1996) apply reaction analysis to arrive at the parameters $A = 33884$ s^{-1} and $E/R = 8304$ K. The rate as a function of temperature using these parameters is shown as Fig. 2.4.

2.3.2 Surface Reaction Submodel

After the particle has been reduced to char, a surface reaction begins, which consumes the combustible fraction, f_{comb}, of the particle. In this work, the wood contains no ash, so that $f_{\mathrm{comb}} + f_{v0} = 1$. The surface reaction mechanism is usually assumed to include two one-step, irreversible reactions (Tillman, 1991):

$$\mathrm{C} + \mathrm{O_2} \rightarrow \mathrm{CO_2} \tag{2.3a}$$

$$\mathrm{C} + 0.5\mathrm{O_2} \rightarrow \mathrm{CO} \tag{2.3b}$$

In general, which reaction dominates depends on whether the char combustion rate is limited by the diffusion of oxygen through the boundary layer surrounding the particle, or by the kinetic rate of the carbon oxidation reactions; (2.3b) is expected to dominate at higher temperatures (Tillman,

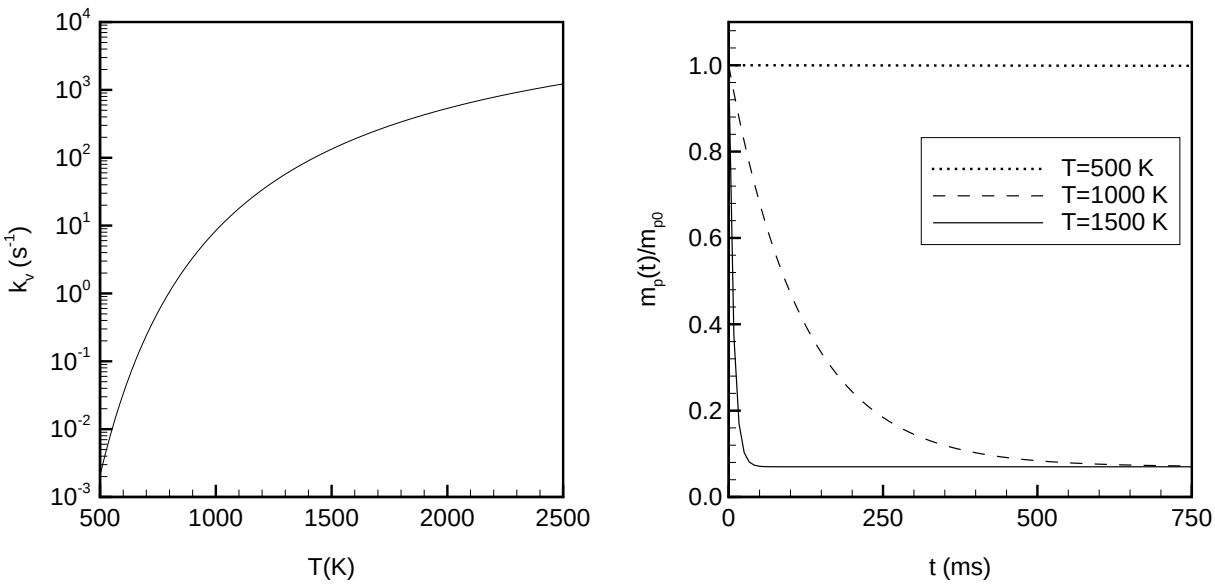

Figure 2.4: Devolatilization rate (left panel) and fraction of the particle mass not devolatilized versus time for various temperatures (right panel).

1991). In FLUENT, it is required that *either* (2.3a) *or* (2.3b) be designated as the surface reaction mechanism, and in this work (2.3a) is used. This choice is made based on the following discussion of the surface reaction model and the simulation results showing that the particles tend to stay in the relatively cool outer region of the combustor (see §3.1).

In FLUENT, three models are available for heterogeneous surface reaction rates: a diffusion-limited model, a kinetics/diffusion-limited model, and the "intrinsic model" of Smith (1982). In this work, the kinetics/diffusion-limited model (Field, 1969; Baum and Street, 1971) is used in which the reaction rate is determined by assuming two resistances in series. The diffusion rate is:

$$R_1 = C_1 \frac{\left[\left(T_p + T_\infty\right)/2\right]^{0.75}}{D_p}\,, \tag{2.4}$$

and the kinetic rate is:

$$R_2 = C_2 \exp(-E/RT_p)\,, \tag{2.5}$$

which, through the parameters C_2 and E, incorporates the effects of chemical reaction on the internal surface of the char particle (intrinsic reaction) and pore diffusion. The resulting rate

Table 2.1: Parameters affecting the surface reaction rate submodel.

Property	Description	Value	Reference
$C1$	mass diffusion limited rate constant	5×10^{-12}	FLUENT
$C2$	kinetics limited rate pre-exponential factor	2×10^{-3}	FLUENT
E	kinetics limited rate activation energy	7.9×10^{-7}j/kgmol	FLUENT
f_{comb}	fraction of the initial particle that will react in a surface reaction	7 %	Malte et al. (1996)
f_h	fraction of reaction heat given to solid	30%	Boyd and Kent (1986)
r	mass of oxidant per mass of char in the particle for complete burnout	2.67	Eqn. (2.3a).

equation is

$$\frac{dm_p}{dt} = -\pi D_p^2 P_O \frac{R_1 R_2}{R_1 + R_2} \,. \tag{2.6}$$

In these equations, T_p is the particle temperature, T_∞ is the local fluid temperature, D_p is the particle diameter, m_p is the instantaneous mass of the particle, and P_O is the partial pressure of the oxidant species in the gas surrounding the combusting particle.

During char combustion, the surface reaction consumes the oxidant species in the gas phase and provides heat and product species to the gas phase. Part of the heat produced by the char reaction is absorbed by the char particle, and is denoted f_h. For oxidation of coal char to CO_2, it is recommended that $f_h = 0.3$ (Boyd and Kent, 1986), and this value is used here for wood char.

The values used in the current simulations for parameters affecting the char combustion rate are given in Table 2.1. To demonstrate the behavior of the surface reaction model with these values applied, the values of R_1, R_2, and R_3=$R_1 R_2/(R_1 + R_2)$ are plotted in Fig. 2.5 for two different particle sizes that are in the range used in the simulations. In the plots, it is assumed that $T_p = T_\infty$. For small particles (50μm), the surface reaction is limited by kinetics at all temperatures, while diffusion is the limiting mechanism for large particles (500μm) at high temperatures.

2.4 Gas-phase Mixing and Reaction

In Reynolds averaged Navier Stokes (RANS) simulations, the time-averaged momentum transport equations are closed by modeling the momentum flux terms (Reynolds stresses). This approach achieves some success because the turbulent velocity fluctuations are driven by the flux of energy out of the mean flow, and the closure models, presumably, need only predict the dissipation of

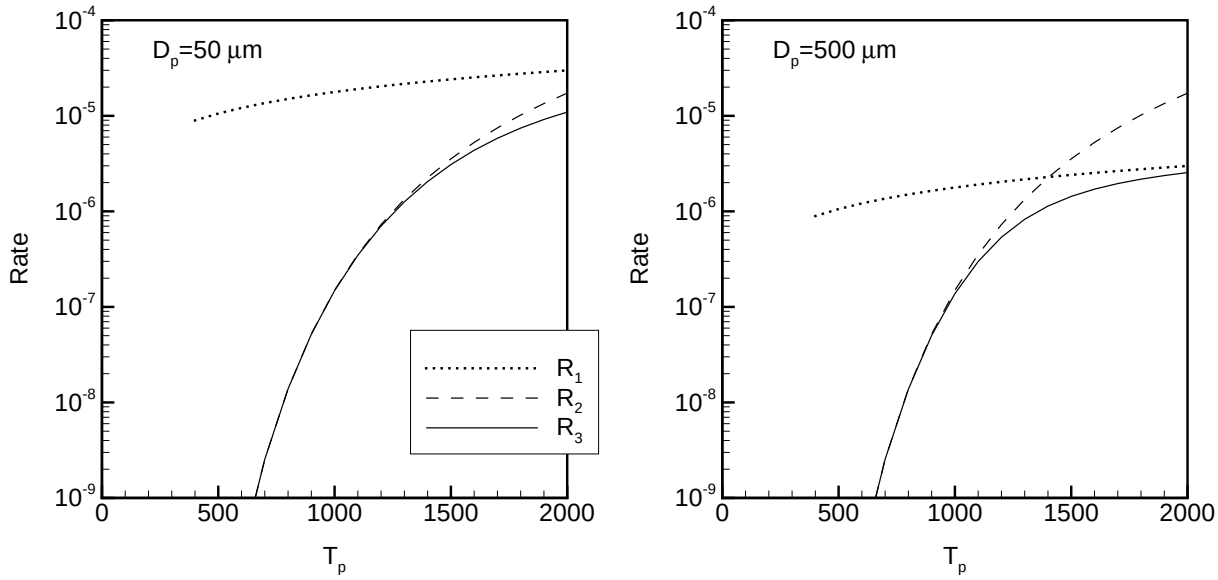

Figure 2.5: Behavior of the kinetic/diffusion surface reaction model for two particle sizes.

this energy reasonably well. In non-premixed reacting flows, however, the local, time-dependent mixing and chemical reaction of the species, and the transfer of heat away from the reaction zone, determine the course of the combustion process. Therefore, the non-linear terms in the reacting species transport equations cannot be modeled in a manner analogous to the modeling used for the flow equations. Instead, three other methods have been proposed for predicting species concentrations in RANS simulations of non-premixed combustion: (1) probability density function (pdf) methods, (2) mixture fraction methods, and (3) the eddy dissipation model.

In the pdf approach (Pope, 1985), a transport equation is solved for the joint probability density of the three components of the velocity and of the composition variables (species mass fractions and enthalpy). The advantage of this method is that the nonlinear terms (the convection terms and the reaction source terms) in the pdf equation are exact and no modeling is required. The disadvantage is that the equation is a function of many independent variables, and Monte Carlo methods are usually employed to solve it. While this approach is generally too computationally intensive for industrial problems and is not available in FLUENT, it is worthwhile mentioning here because it is sometimes confused with the mixture fraction method, discussed next, in which a form for the pdf of the fluctuations in a conserved scalar is assumed.

In the mixture fraction approach, it is assumed that the amount of reaction that occurs be-

tween two initially segregated streams (a fuel stream and an oxidizer stream) can be predicted if the amount of mixing of the two streams is known. This assumption is good for non-premixed combustion with moderate to high Damköhler number. The mixing between the fuel and oxidizer streams is calculated by solving the transport equation for a conserved scalar, ξ, which has the value of 0 in the oxidizer stream and 1 in the fuel stream. The conserved scalar is termed the "mixture fraction." In RANS, a transport equation is solved for the time-averaged mixture fraction, and the time dependent ξ is modeled. A common approach to modeling ξ is to solve a transport equation for the variance of ξ and assume a beta pdf for the fluctuations (see 2.5.3).

In the eddy dissipation model, transport equations are solved for each reacting species of interest. The reaction source terms are modeled using the technique of Magnussen and Hjertager (1976), in which the turbulence kinetic energy and its dissipation rate are used to estimate the effects of turbulence on the reaction rates. With this method, only a small number of species can be considered due to limited computer capacity, and the chemical kinetics must be modeled through a reduced reaction mechanism. The mechanism used in this work is discussed in 2.4.1. As discussed in Chapter 3.2, the reaction rate in the McConnell burner is limited by the mixing rate in most locations, and so it is likely that the mixture fraction approach will be effective for predicting the mass fractions in this flow. There are several numerical advantages of the mixture fraction approach over the eddy dissipation model. First, only two scalar transport equations must be solved, as opposed to one for each species, and so the simulation requires less time per iteration. Second, by eliminating the reacting species equations from the simulation, the highly non-linear reaction rate terms are eliminated, so that the simulation converges in significantly fewer iterations. Third, since the number of transport equations is not related to the number of species, the mass fractions for a large number of species can be efficiently computed.

2.4.1 Reduced Finite Rate Mechanism

In simulations in which the eddy dissipation model is used, only a small number of reacting species transport equations can be solved practically. Therefore, the full finite rate reaction mech-

anism must be represented by a reduced mechanism. The reduced mechanism used in this work is discussed in this section.

In the simulations, the wood particles are considered to break down during the devolatilization process into char, which contains only carbon,[1] and wood volatiles; the volatiles are considered to be released from the wood as a single species which undergoes further reaction. In the current simulations, the composition of the wood particles is taken to be $C_6H_{9.36}O_{3.97}N_{0.0107}$, 93% of which by mass becomes wood volatiles (Malte et al., 1996). Therefore, wood volatiles have the composition $CH_{1.816}O_{0.770}N_{0.00208}$. The volatiles undergo very fast spontaneous decomposition

$$\begin{aligned} &CH_{1.816}O_{0.770}N_{0.00208} \rightarrow \\ &\qquad 0.4141CO + 0.2071H_2O + 0.07451CO_2 + 0.1895CH_4 + 0.1609C_2H_4 + 0.00104N_2 \ , \end{aligned} \tag{2.7}$$

the products of which react according to the following mechanism:

$$CH_4 + \frac{3}{2}O_2 \rightarrow CO + 2H_2O \qquad R = 10^{9.45} \exp\left(\frac{-24358}{T}\right) [CH_4]^{-0.3}[O_2]^{1.3} \tag{2.8}$$

$$CO + \frac{1}{2}O_2 \rightarrow CO_2 \qquad R = 10^{12.35} \exp\left(\frac{-20131}{T}\right) [CO]^{1.0}[H_2O]^{0.5}[O_2]^{0.25} \tag{2.9}$$

$$CO_2 \rightarrow CO + \frac{1}{2}O_2 \qquad R = 10^{8.70} \exp\left(\frac{-20131}{T}\right) [CO_2]^{1.0} \tag{2.10}$$

$$C_2H_4 + 3O_2 \rightarrow 2CO_2 + 2H_2O \qquad R = 10^{10.05} \exp -15106T[C_2H_4]^{0.1}[O_2]^{1.65} \ . \tag{2.11}$$

In the above mechanism, the first three reaction rates are those of Westbrook and Dryer (1984) for a reduced methane-air reaction, while the fourth rate uses the default values in FLUENT for a one-step ethylene-air reaction. The mole numbers of the products in (2.7) are determined in Malte et al. (1996) based the literature and on a laboratory study of wood devolatilization at a fast rate.

2.5 NO_x Production

Oxides of nitrogen (NO_x) include nitric oxide (NO), nitrogen oxide (NO_2). Since these species are involved in a number of reactions during typical turbulent combustion, predicting NO_x concentrations using numerical simulations requires extensive modeling. In this section, the thermal

[1] During post-processing to compute pollutant formation, the char may be considered to contain a small amount of nitrogen. The amount of nitrogen that remains in the char has an insignificant effect on the evolution of the major species, and so complete devolatilization of the nitrogen is assumed during the simulations.

(Zeldovich) mechanism involving atmospheric nitrogen and a mechanism by which NO_x is formed by oxidation of nitrogen in the fuel are considered. Other paths by which NO_x can be produced, e.g., Fenimore (prompt) mechanism, N_2O-intermediate mechanism, NNH mechanism, are not considered in the current work.

Typically in RANS simulations, and in FLUENT in particular, NO_x concentrations are predicted by post-processing data from reacting flow simulations. This method can be used because NO_x concentrations are so small that reactions involving NO_x have no significant effect on the concentrations of the major species or on the temperature of the flow field, i.e., the NO_x reactions can be decoupled from the rest of the flow calculation. For thermal NO_x calculations, the transport equation for NO is solved (using the appropriate RANS closure model for the convective term), and for fuel NO_x calculations the transport equation for HCN is also involved; these equations are included here for completeness.

$$\rho\frac{\partial Y_{\mathrm{NO}}}{\partial t} + \rho u_i \frac{\partial Y_{\mathrm{NO}}}{\partial x_i} = \frac{\partial}{\partial x_i}\left(\rho\mathcal{D}\frac{\partial Y_{\mathrm{NO}}}{\partial x_i}\right) + S_{\mathrm{NO}} \tag{2.12}$$

$$\rho\frac{\partial Y_{\mathrm{HCN}}}{\partial t} + \rho u_i \frac{\partial Y_{\mathrm{HCN}}}{\partial x_i} = \frac{\partial}{\partial x_i}\left(\rho\mathcal{D}\frac{\partial Y_{\mathrm{HCN}}}{\partial x_i}\right) + S_{\mathrm{HCN}}\ . \tag{2.13}$$

Here, Y_{NO} and Y_{HCN} are mass fractions of NO and HCN; S_{NO} and S_{HCN} are to the source terms which are modeled as described below.

2.5.1 Thermal NO_x

The formation of thermal NO_x is described by three chemical reactions known as the extended Zeldovich mechanism:

$$\mathrm{O} + \mathrm{N_2} \overset{k_1}{\Longleftrightarrow} \mathrm{N} + \mathrm{NO} \tag{2.14}$$

$$\mathrm{N} + \mathrm{O_2} \overset{k_2}{\Longleftrightarrow} \mathrm{O} + \mathrm{NO} \tag{2.15}$$

$$\mathrm{N} + \mathrm{OH} \overset{k_3}{\Longleftrightarrow} \mathrm{H} + \mathrm{NO} \tag{2.16}$$

The rate constants for these reactions have been measured in numerous experimental studies (Blauwens et al., 1977; Flower et al., 1975; Monat et al., 1979). Both FLUENT and Turns (2000) use the values compiled by Hanson and Salimian (1984):

$$k_1 = 1.8 \times 10^8 \exp\left(\frac{-38370}{T}\right) \qquad \mathrm{m^3\ mol^{-1}\ s^{-1}} \tag{2.17}$$

$$k_{-1} = 3.8 \times 10^7 \exp\left(\frac{-425}{T}\right) \qquad \mathrm{m^3\ mol^{-1}\ s^{-1}} \tag{2.18}$$

$$k_2 = 1.8 \times 10^4 T \exp\left(\frac{-4680}{T}\right) \qquad \mathrm{m^3\ mol^{-1}\ s^{-1}} \tag{2.19}$$

$$k_{-2} = 3.8 \times 10^3 T \exp\left(\frac{-20820}{T}\right) \qquad \mathrm{m^3\ mol^{-1}\ s^{-1}} \tag{2.20}$$

$$k_3 = 7.1 \times 10^7 \exp\left(\frac{-450}{T}\right) \qquad \mathrm{m^3\ mol^{-1}\ s^{-1}} \tag{2.21}$$

$$k_{-3} = 1.7 \times 10^8 \exp\left(\frac{-24560}{T}\right) \qquad \mathrm{m^3\ mol^{-1}\ s^{-1}} \tag{2.22}$$

In the above expressions, k_1, k_2, and k_3 are the rate constants for the forward reactions (2.14)–(2.16), respectively, and k_{-1}, k_{-2}, and k_{-3} are the corresponding reverse rates. The net rate of formation of NO via the Zeldovich mechanism is then

$$\begin{aligned} \frac{d[\mathrm{NO}]}{dt} &= k_1[\mathrm{O}][\mathrm{N_2}] + k_2[\mathrm{N}][\mathrm{O_2}] + k_3[\mathrm{N}][\mathrm{OH}] - k_{-1}[\mathrm{NO}][\mathrm{N}] \\ &- k_{-2}[\mathrm{NO}][\mathrm{O}] - k_{-3}[\mathrm{NO}][\mathrm{H}] \end{aligned} \tag{2.23}$$

where all concentrations have units mol/m^3. In order to calculate the formation rates of NO, the concentrations of N, N_2, O, H, and OH must be either known or modeled.

To develop a model for [N], it is noted that the activation energy for (2.14) is relatively high (319,050 kJ/kmol) so that the reaction is highly temperature dependent and relatively slow, except at very high temperatures (Turns, 2000). The activation energy for oxidation of N atoms, on the other hand, is small. Therefore, the reaction time scale for the oxidation of N is much shorter than the time scale of (2.14) so that, provided there is sufficient oxygen (non-rich combustion), [N] will be in steady-state. With this assumption, the NO formation rate becomes

$$\frac{d[\mathrm{NO}]}{dt} = 2k_1[\mathrm{O}][\mathrm{N}_2]\frac{\left(1 - \frac{k_{-1}k_{-2}[\mathrm{NO}]^2}{k_1[\mathrm{N}_2]k_2[\mathrm{O}_2]}\right)}{\left(1 + \frac{k_{-1}[\mathrm{NO}]}{k_2[\mathrm{O}_2]+k_3[\mathrm{OH}]}\right)} \quad (\mathrm{mol/m^3s}) \tag{2.24}$$

Temperature and the remaining unknown species concentrations ([O_2], [N_2], [O], and [OH]) can be treated by decoupling the fuel combustion chemistry from the reactions involving thermal NO_x. This approximation is reasonable since, in typical combustion processes, the fuel combustion is complete before NO formation can become significant, NO_x concentrations are very small, and the heat released by the NO_x reactions is insignificant. Therefore, in numerical simulations in which [O_2], [N_2], [O], and [OH] are calculated directly in the solution of the fuel chemistry mechanism, the computed values are applied as constants in (2.24). In the current simulations in which the kinetic mechanism of §2.4.1 is used, [O], and [OH] are not known and so the equilibrium chemistry values are assumed. It is noted that Bilger and Beck (1975) suggest that in turbulent diffusion flames, the assumption of equilibrium O atom concentration is inaccurate, but this issue is not considered in the current work. In summary, the contribution of thermal NO_x production to the source term in (2.12) is

$$S_{\mathrm{thermal,NO}} = M_{\mathrm{NO}}\frac{d[\mathrm{NO}]}{dt} \tag{2.25}$$

where M_{NO} is the molecular weight of NO, and $d[\mathrm{NO}]/dt$ is computed from (2.24).

2.5.2 Fuel NO_x

Wood contains approximately 0.1 % nitrogen by weight, and samples of wood and resin dust analyzed by Malte et al. (1996) contained 5.65 % nitrogen by weight. Assuming complete conversion of fuel nitrogen to NO_x, wood dust and wood/resin dust would yield 102 and 5399 parts per million on a dry volume basis adjusted to 15% O_2 (ppmvd), respectively. While full conversion of fuel

Pathway #1 (Smoot and Smith, 1985)

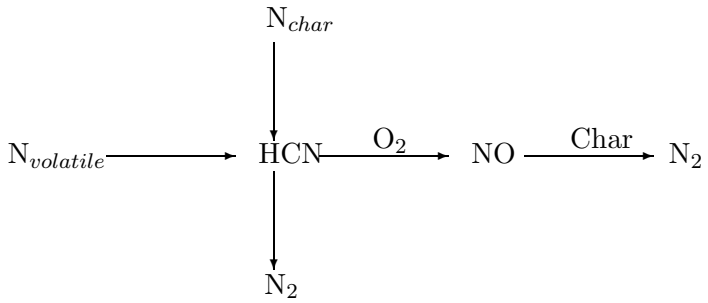

Pathway #2 (Lockwood and Romo-Millanes, 1992)

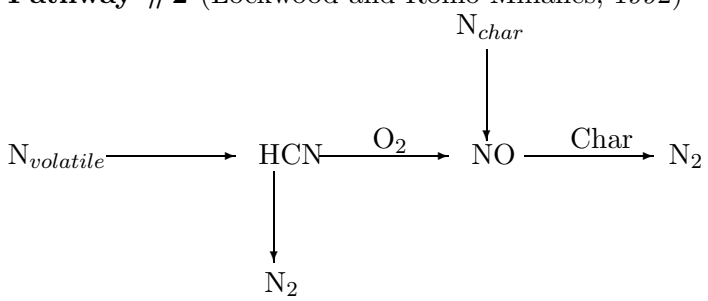

Figure 2.6: Pathways for the production of fuel-NO_x.

nitrogen is not expected to occur in the McConnell burner, significant concentrations of fuel NO_x may be produced in the burner and must be accounted for in the simulations. Models for fuel-NO_x production are discussed in this section. The discussion is based on the assumption that the mechanisms by which NO_x is formed from nitrogen in wood are similar to those by which it is formed from nitrogen in coal.

When wood particles are heated, some of the fuel-bound nitrogen is released into the gas phase ($N_{volatiles}$) and some remains in the char (N_{char}). Presumably, the bulk of the fuel-nitrogen in wood devolatilizes, but a model for fuel-NO_x production should account for both $N_{volatiles}$ and N_{char}. For coal combustion, two pathways have been suggested; they are shown graphically in Fig. 2.6. In both model pathways, the nitrogen released as gas is assumed to form HCN; research by Leppälahti and Koljonen (1995) and Aho et al. (1993) indicate that this assumption is a good one for wood combustion. The HCN is then either oxidized to NO or reduced to N_2. The two model pathways, however, differ in the treatment of N_{char}. Smoot and Smith (1985) assume that N_{char} forms HCN; this simplifies the modeling in that no assumption must be made as to what fraction of the fuel nitrogen is released as gas in the devolatilization phase. Lockwood and Romo-Millanes (1992) assume that N_{char} competes for oxygen with the carbon in the char and oxidizes to NO. In our discussion of char oxidation (§2.3.2), we note that carbon can be assumed to oxidize to CO_2

or to CO depending if the reaction is kinetics or oxygen limited. Presumably, the model for the fate of N_{char} should be consistent with the char oxidation model, i.e., the Smoot and Smith (1985) approach should be used if it is assumed that the oxidation of carbon in the char is limited by the diffusion of oxygen through the boundary layer.

From the diagrams of the model pathways, it is apparent that multiple mechanisms affect the concentrations of HCN and NO. In the simulations, these mechanisms are accounted for through source terms in the transport equations (2.12) and (2.13):

$$S_{\mathrm{HCN}} = S_{\mathrm{pvc,HCN}} + S_{\mathrm{HCN-1}} + S_{\mathrm{HCN-2}} \tag{2.26}$$

$$S_{\mathrm{NO}} = S_{\mathrm{C,NO}} + S_{\mathrm{NO-1}} + S_{\mathrm{NO-2}} + S_{\mathrm{NO-3}} \tag{2.27}$$

The nomenclature is explained in the discussions which follow.

HCN Depletion

HCN is depleted through oxidation to NO or reduction to N_2. Denoting these reactions with the subscripts 1 and 2, respectively, the rates of conversion of HCN are given by de Soete (1975) as

$$R_1 = A_1 \; X_{\mathrm{HCN}} \; X_{\mathrm{O_2}}^{a} \; \exp(-E_1/RT) \tag{2.28}$$

$$R_2 = A_2 \; X_{\mathrm{HCN}} \; X_{\mathrm{NO}} \; \exp(-E_2/RT) \tag{2.29}$$

where

R_1, R_2	=	destruction rates of HCN (1/s)
T	=	instantaneous temperature (K)
X	=	mole fractions
A_1	=	3.5×10^{10} 1/s
A_2	=	3.0×10^{12} 1/s
E_1	=	67000 cal/mol
E_2	=	60000 cal/mol

The oxygen reaction order a depends on flame conditions. According to de Soete (1975), oxygen reaction order is uniquely related to oxygen mole fraction in the flame:

$$a = \begin{cases} 1.0, & X_{O_2} \leq 4.1 \times 10^{-3} \\ -3.95 - 0.9 \ln X_{O_2}, & 4.1 \times 10^{-3} \leq X_{O_2} \leq 1.11 \times 10^{-2} \\ -0.35 - 0.1 \ln X_{O_2}, & 1.11 \times 10^{-2} < X_{O_2} < 0.03 \\ 0, & X_{O_2} \geq 0.03 \end{cases} \tag{2.30}$$

Since mole fraction is related to mass fraction through molecular weights of the species (M_i) and the mixture (M_m),

$$X_i = Y_i \frac{M_m}{M_i} = \frac{Y_i}{M_i} \left(\frac{\rho RT}{P} \right) \ . \tag{2.31}$$

It follows, then, that the mass consumption rates of HCN which appear in (2.26) are calculated as

$$S_{\mathrm{HCN}-1} = -R_1 \frac{M_{\mathrm{HCN}} P}{RT} \tag{2.32}$$

$$S_{\mathrm{HCN}-2} = -R_2 \frac{M_{\mathrm{HCN}} P}{RT} \tag{2.33}$$

where P is the pressure (Pa), and R is the universal gas constant. The sources in (2.27) are evaluated as

$$S_{\mathrm{NO}-1} = -S_{\mathrm{HCN}-1} \frac{M_{\mathrm{NO}}}{M_{\mathrm{HCN}}} = R_1 \frac{M_{\mathrm{NO}} P}{RT} \tag{2.34}$$

$$S_{\mathrm{NO}-2} = S_{\mathrm{HCN}-2} \frac{M_{\mathrm{NO}}}{M_{\mathrm{HCN}}} = -R_2 \frac{M_{\mathrm{NO}} P}{RT} \tag{2.35}$$

HCN Production and NO Production from Char

In the models for the production of fuel NO_x, HCN is produced from from nitrogen in the volatiles and may be produced from nitrogen in the char. The overall source of HCN ($S_{\mathrm{pvc,HCN}}$) is the sum of the two contributions, i.e.,

$$S_{\mathrm{pvc,HCN}} = S_{\mathrm{V,HCN}} + S_{\mathrm{C,HCN}} \tag{2.36}$$

The source of HCN from the volatiles is related to the rate of volatile release:

$$S_{\mathrm{V,HCN}} = S_{\mathrm{V}} Y_{\mathrm{NV}} \frac{M_{\mathrm{HCN}}}{M_{\mathrm{N}}} \tag{2.37}$$

where

S_{V} = rate of volatile production ($\mathrm{kg/m^3 \cdot s}$)

Y_{NV} = mass fraction of nitrogen in the volatiles

M_{HCN}, M_{N} = molecular weight of HCN and N

Calculation of sources related to char-bound nitrogen depends on the fuel $\mathrm{NO_x}$ pathway model. With the first pathway model, all N_{char} converts to HCN. Thus,

$$S_{\mathrm{C,HCN}} = S_C Y_{\mathrm{NC}} \frac{M_{\mathrm{HCN}}}{M_{\mathrm{N}}} \tag{2.38}$$

$$S_{\mathrm{C,NO}} = 0 \tag{2.39}$$

where

S_C = char burnout rate ($\mathrm{kg/m^3 \cdot s}$)

Y_{NC} = mass fraction of nitrogen in char

With the second pathway model, the char nitrogen is released to the gas phase as NO directly. If this approach is followed, then

$$S_{\mathrm{C,HCN}} = 0 \tag{2.40}$$

$$S_{\mathrm{C,NO}} = S_C Y_{\mathrm{NC}} \frac{M_{\mathrm{NO}}}{M_{\mathrm{N}}} \tag{2.41}$$

NO Reduction on the Char Surface

The heterogeneous reaction in which NO reduction occurs on the char surface is modeled as by Levy et al. (1981). It is an adsorption reaction the rate of which is directly proportional to the pore surface area. The pore surface area is also known as the "BET surface area" due to the researchers who pioneered the adsorption theory (Brunauer, 1943). For coal, the BET area is typically 25,000 $\mathrm{m^2/kg}$, and we use this value for wood char unless otherwise noted. The reaction rate is modeled as

$$R_3 = A_3 \exp(-E_3/RT)\overline{P}_{\mathrm{NO}} \tag{2.42}$$

where

R_3 = rate of NO reduction ($\mathrm{mole/s/m^2_{BET}}$)

$\overline{P}_{\mathrm{NO}}$ = mean NO partial pressure (atm)

E_3 = 34,100 cal/mol

A_3 = 230 $\mathrm{mole/atm/m^2_{BET}/s}$

The partial pressure $\overline{P}_{NO}$ is calculated using Dalton's law: $P_{\mathrm{NO}} = X_{\mathrm{NO}}P$. It follows that the rate of NO consumption due to reaction with the char is

$$S_{\mathrm{NO}-3} = A_{\mathrm{BET}} c_s M_{\mathrm{NO}} R_3/1000 \tag{2.43}$$

where

$$\begin{aligned} A_{\mathrm{BET}} &= \text{BET surface area } (\mathrm{m}^2/\mathrm{kg}) \\ c_s &= \text{concentration of particles } (\mathrm{kg}/\mathrm{m}^3) \\ S_{\mathrm{NO}-3} &= \text{NO consumption } (\mathrm{kg}/\mathrm{m}^3/\mathrm{s}) \end{aligned}$$

2.5.3 The Effects of Turbulent Fluctuations

In the foregoing discussions of models for thermal and fuel $\mathrm{NO_x}$ production, the instantaneous values for species mass fractions and temperature have been used. In Reynolds Averaged Navier Stokes simulations of reacting flows, however, it is the Favre averaged transport equations that are solved, and the instantaneous variables are not available. Since the relationships among $\mathrm{NO_x}$ formation rate, temperature, and species concentration are nonlinear, the instantaneous quantities must be modeled. In general, two approaches are used for this purpose: (1) moment methods Williams (1975), and (2) assumed PDF methods. The latter approach is used in FLUENT.

While the exact form of the modeling for species and temperature fluctuations depends on the approach used to close the species transport equations (mixture fraction method or the eddy dissipation model, the Favre averaged reaction rate for the i_{th} species is

$$\overline{w_i} = \int \cdots \int w_i(V_1, V_2, \ldots) P(V_1, V_2, \ldots) dV_1 \; .dV_2 \ldots \tag{2.44}$$

where V_1, V_2, ... are temperature and species concentrations. P is the probability density function (PDF). In FLUENT, it is assumed that V_1, V_2, ... are statistically independent so that the joint probability density of several variables can be expressed as the product of the probability density of each variable, i.e., for two variables

$$P(V_1, V_2) = P_1(V_1) P_2(V_2) \tag{2.45}$$

Next, P is modeled as a two-moment beta function

$$P(V) = \frac{\Gamma(\alpha+\beta)}{\Gamma(\alpha)\Gamma(\beta)} V^{\alpha-1}(1-V)^{\beta-1} = \frac{V^{\alpha-1}(1-V)^{\beta-1}}{\int_0^1 V^{\alpha-1}(1-V)^{\beta-1} dV} \tag{2.46}$$

where $\Gamma(\cdot)$ is the Gamma function, α and β depend on m, the mean value of the quantity in question, and its variance, σ^2:

$$\alpha = m\left(\frac{m(1-m)}{\sigma^2} - 1\right) \tag{2.47}$$

$$\beta = (1-m)\left(\frac{m(1-m)}{\sigma^2} - 1\right) \tag{2.48}$$

The beta function requires that the independent variable V assume values between 0 and 1. Thus, field variables such as temperature must be normalized. Finally, σ^2 is modeled by solving an approximate transport equation:

$$\frac{\partial}{\partial t}\left(\rho\sigma^2\right) + \frac{\partial}{\partial x_i}\left(\rho u_i \sigma^2\right) = \frac{\partial}{\partial x_i}\left(\frac{\mu_t}{\sigma_t}\frac{\partial \sigma^2}{\partial x_i}\right) + C_g \mu_t \left(\frac{\partial m}{\partial x_i}\right)^2 - C_d \rho \frac{\epsilon}{k}\sigma^2 \tag{2.49}$$

where the constants σ_t, C_g and C_d take the values 0.7, 2.86, and 2.0, respectively. Assuming equal production and dissipation of variance, one gets

$$\sigma^2 = \frac{\mu_t}{\rho}\frac{k}{\epsilon}\frac{C_g}{C_d}\left(\frac{\partial m}{\partial x_i}\right)^2 = \frac{\mu_t}{\rho}\frac{k}{\epsilon}\frac{C_g}{C_d}\left[\left(\frac{\partial m}{\partial x}\right)^2 + \left(\frac{\partial m}{\partial y}\right)^2 + \left(\frac{\partial m}{\partial z}\right)^2\right] \tag{2.50}$$

The term in the brackets is the dissipation rate of the independent variable.

Chapter 3

Numerical Simulations

In the previous chapter, several models were presented for the various aspects of the fluid dynamics and chemical reaction in the McConnell burner. In order to examine the ffects of these models in a systematic manner, multiple simulations have been run; they are summarized in Table 3.1. In the first three simulations, designated by the letter "M" to indicate that the fuel considered is methane, the closure models for the Navier-Stokes equations are examined in conjunction with a relatively simple and well understood one-step global reaction mechanism for methane reacting with air. In the remaining simulations, designated by "W" for wood, the Reynolds stress model is used to close the momentum transport equations; in simulation W1, the constituents of wood volatiles are injected into the burner in the gas phase along with char particles, while in W2, no gas phase fuel is injected and the fuel is wood dust. The fuel-air equivalence ratio (ϕ) is adjusted in simulation W1 to approximately match the exit plane temperature in W1 and W2 by accounting for the difference in enthalpy of formation between wood volatiles and the individual species that make up the volatiles.

Table 3.1: Summary of the simulations.

	Gaseous fuel	Solid fuel	Gas-phase reactions	Turbulence model	ϕ
M1	CH_4		one-step	k-ε	0.45
M2	CH_4		one-step	RNG	0.45
M3	CH_4		one-step	RSM	0.45
W1	CO, CH_4, C_2H_4, H_2O, CO_2	char	(2.8)-(2.11)	RSM	0.40
W2		wood	(2.7)-(2.11)	RSM	0.46

3.1 Hydrodynamic Validation

There are no measurements available of the flow field in the burner, so direct validation of the simulations is not presently possible. The manufacturer does report the static pressure at the discharge of the air blower, however, and the velocity field can be evaluated for plausibility. For reference, various statistics from the flow fields are presented in Table 3.2.

We begin the discussion of the hydrodynamics by observing a transverse cut through the velocity field at the axial midpoint of the burner, which is displayed in Fig. 3.1. The top and bottom panels in the figure are from simulations M3 and M1 respectively. Both the models predict an outer vortex that rotates with little shear surrounding an inner region of high angular velocity and high shear. The RSM predicts a higher angular velocity for the core flow than does the k-ϵ model. Since a strongly swirling flow is indicated, the Reynolds stresses are expected to be anisotropic; the ratios of the stresses presented in Table 3.2 show this to be the case.

Also presented in Table 3.2 are the static pressure at the tuyéres (P_{in}) and the drop in total pressure across the burner (ΔP_{tot}). All three turbulence models predict comparable inlet pressure and pressure losses with the values from the RSM midway between the two variants of k-ϵ. From the manufacturer's inlet pressure data, the maximum possible drop in total pressure across the actual burner is about 35 inches of water (8700 Pa), and all the models yield results that are consistent with this. The total pressure on a longitudinal cut through the centerline is shown in Fig. 3.2 for the RSM and k-ϵ model. While the overall drop in total pressure is comparable in the two simulations, the contour plots show that the locations in the burner where total pressure is lost are different. Since total pressure is lost due to viscous shearing, and viscous shearing causes mixing of heat and species, differences in the total pressure field imply differences in mixing.

From the pressure and velocity data, it is apparent that the three turbulence models yield generally similar predictions for the flow field, but that the predictions differ in some details. One

Table 3.2: Summary of hydrodynamic data. $\langle\ \rangle$ indicate spatial averages over the computational domain.

	P_{in} (Pa gage)	ΔP_{tot} (Pa)	$\langle\overline{uu}\rangle$ / $\langle\overline{vv}\rangle$	$\langle\overline{uu}\rangle$ / $\langle\overline{ww}\rangle$	y^+_{max}
M1	16317	8612	–	–	2291
M2	12535	8068	–	–	3178
M3	15182	8200	1.39	1.47	3343
W1	15196	8104	1.30	1.41	3357
W2	15184	8185	1.28	1.42	2817

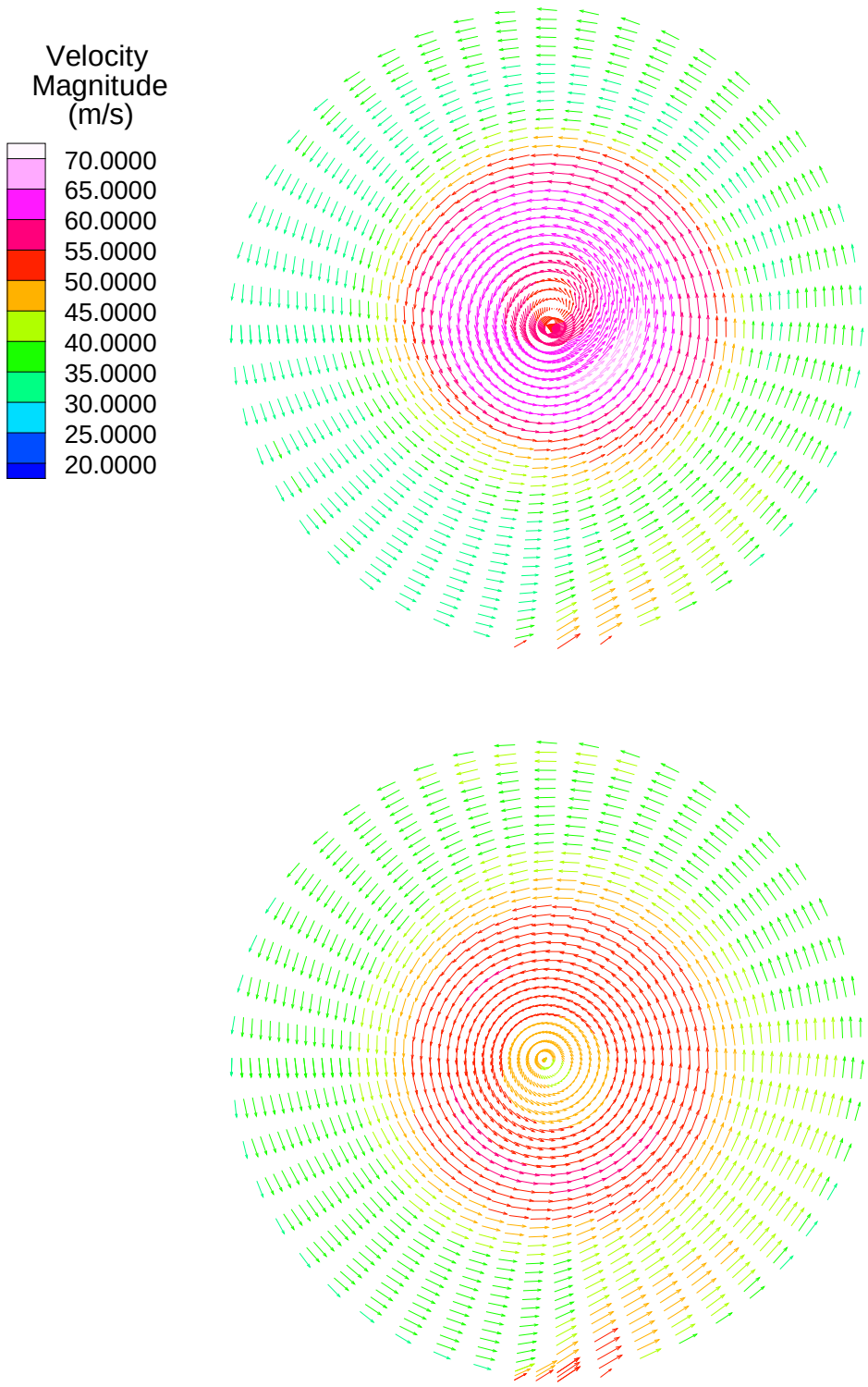

Figure 3.1: Velocity magnitude (m/s) at the midplane. The top panel is with RSM modeling, the bottom with KE modeling.

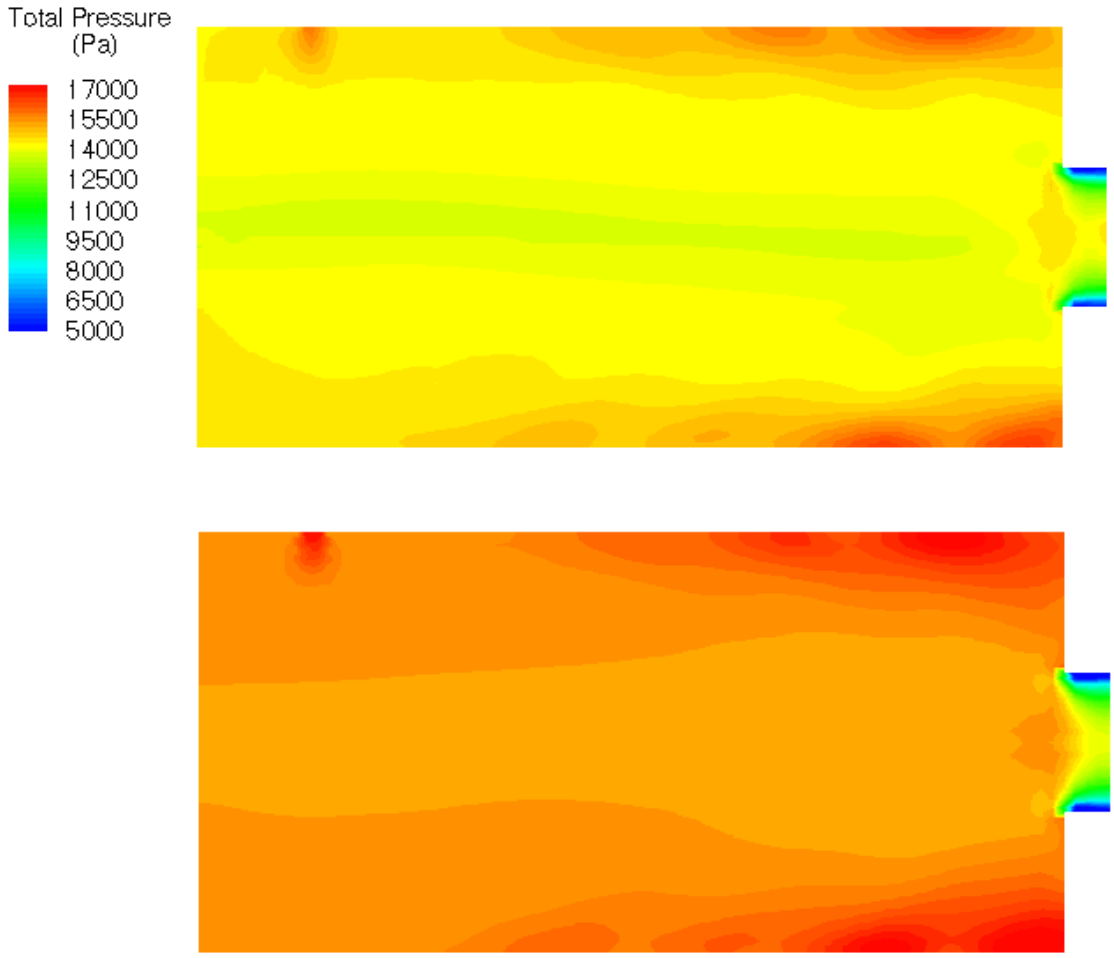

Figure 3.2: Total pressure (Pa) on the vertical centerline plane with fuel entering from the top. The top panel is with RSM modeling, the bottom with KE modeling.

detail that is of particular interest in studies of non-premixed turbulent combustion is the local strain rate, since shearing determines the rate of mixing, which affects the rate of chemical reaction. From the plots of velocity and total pressure, it is apparent that k-ϵ, RNG (not shown), and RSM yield different predictions for the size and location of the region of high shear inside the outer vortex, and the question is which model most closely predicts the flow in the physical burner. An examination of the derivations of the three turbulence models indicates that, if any of them can yield good predictions, it is the RSM. As in most two equation turbulence models, an assumption inherent in the k-ϵ and RNG models is that of Boussinesq (1877), i.e., that the Reynolds-stress tensor can be related to the mean strain-rate tensor by an eddy viscosity. Wilcox (1993) notes that among the applications for which this modeling assumption is not valid are flow over curved surfaces, flow in rotating and stratified fluids, and three-dimensional flow; therefore, k-ϵ and RNG are not expected to be effective for the current flow. Several researchers who have studied the simulation of confined vortices and cyclonic combustors conclude that eddy-viscosity based models are not appropriate for these flows (Boysan et al., 1986; Hogg and Leschziner, 1989a,b; Zhang and Nieh, 1997). Based on the guidance from these sources, the RSM is used for the simulations involving wood, which are the focus of this research.

3.2 Temperatures and Species Concentrations

In order to use the simulations to predict concentrations of pollutant species such as NO_x, it is first necessary to demonstrate that the predictions for the temperature and major species fields are consistent with available data. Temperature and species data are shown in several formats in Table 3.3 and Figs. 3.3 through 3.5.

We begin by considering exit plane temperatures and species concentrations since these values can be compared with analytically determined limits. In Table 3.3 are shown the average temperatures at the exit plane as predicted by FLUENT. Also shown are the adiabatic flame temperatures assuming equilibrium composition and the fuel-air equivalence ratio (ϕ) used in the simulations.[1] Since the equilibrium composition for the conditions simulated includes insignificant mole fractions of combustion products other than H_2O and CO_2, the adiabatic flame temperature closely approximates the upper limit of the exit plane temperature in the simulations.

[1]The equilibrium values were computed using the UWeq code developed by D. T. Pratt considering fourteen product species: H, HO_2, H_2, H_2O, H_2O_2, O, OH, O_2, CO, CO_2, N_2, N_2O, NO, NO_2.

In all simulations involving methane, the exit plane temperatures are less than the limiting temperature, and the amounts by which they differ from the limit are consistent with the amount of unburned fuel at the exit plane. The peak temperatures slightly exceed the limit predicted by equilibrium analysis, which may be an artifact of the one-step reaction mechanism used in the simulations; the equilibrium calculations take into account the effect the endothermic formation of NO which occurs at high rates when the temperature is greater than 2200 K. In simulation M2, the RNG turbulence model apparently retards mixing to an unrealistic extent; the amount of mixing in M3 is less than that in M1, which is consistent with the excessive turbulent diffusion observed when the k-ϵ model is used for swirling flows (Hogg and Leschziner, 1989a,b). The mass fractions (Y) of H_2O and CO_2 at the exit plane in the simulations involving methane are consistent with the amount of unburned fuel and the exit plane temperatures.

In the simulations involving wood, the exit plane temperatures are slightly less than the prediction by equilibrium methods, which is consistent with the levels of unburned CO, CH_4, and C_2H_4 at the exit; the simulations predict complete burning of the char particles. The peak temperatures observed in simulations W1 and W2 exceed the maximum possible based on equilibrium analysis, but, as with methane, this is most likely an artifact of the reduced reaction set.

In Fig. 3.3 are shown the contours of static temperature on a longitudinal plane for simulations M3 and W2. In both cases, a hot core is surrounded by cool air entering from the downstream tuyéres. In the case of methane, the one-step reaction mechanism dictates heat release only where fuel coexists with a considerable amount of oxidant, and there is a steep temperature gradient where the burning occurs in a conical diffusion flame at the edge of the hot core. In simulation W2, the temperature gradients are less steep and the diffusion flame is less pronounced. This is in part

Table 3.3: Summary of temperatures and species concentrations. The exit values are mass weighted averages at the exit plane.

	Peak T(K)	Exit T(K)	Exit Y_{CO_2}	Exit Y_{H_2O}	Exit Y_{CO}	Exit Y_{CH_4}	Exit $Y_{C_2H_4}$
Equil. CH_4	2225	1378	0.075	0.062	0	0	n/a
M1	2277	1347	0.072	0.059	n/a	1.0×10^{-3}	n/a
M2	2250	1199	0.062	0.051	n/a	9.1×10^{-3}	n/a
M3	2244	1317	0.072	0.058	n/a	1.2×10^{-3}	n/a
Equil. Wood	2136	1199	0.109	0.035	3.4×10^{-9}	n/a	n/a
W1	2012	1158	0.106	0.035	5.3×10^{-3}	1.2×10^{-3}	1.9×10^{-3}
W2	2004	1148	0.105	0.035	5.3×10^{-3}	1.2×10^{-3}	2.0×10^{-3}

due to the presence of significant amounts of CO which, in the context of the reaction mechanism used in the simulations, requires less mixing of fuel and air before reaction begins. The contours of O2 mass fraction (Fig. 3.4) show a core depleted of oxidant, a diffusion zone, and an outer region rich in oxidant. As noted in the preceding paragraph, the profiles for the wood and methane simulations are different, and some of this difference is likely due to the grossly simplified reaction mechanisms assumed in the simulations. In the methane simulation, and to a lesser extent in the wood simulation, little mixing occurs between the core ow and the air entering through the downstream tuyeres. Further investigation of this phenomena is warranted because if it exists in the physical burner (rather than being an artifact of the simulations) it suggests an area in which burner performance may be improved with respect to carbon conversion efficiency. The long, hot central ame, however causes fuel-NOx to be reduced to N_2 (see Chapter 4). The next contour plots are of CO2 mass fraction (Fig. 3.5). Due to the selection of contour spacing, it is especially apparent in this figure that unmixed air from the downstream tuyeres exits the burner. Also evident in the lower panel of the figure are high concentrations of CO_2 upstream in the burner; these result from oxidation of the char particles directly to CO_2. Since the W2 simulation shows oxidant levels to be extremely low in the upstream end of the burner where the char oxidation is occurring, the effect of assuming that the char oxidizes to CO should be evaluated. Finally, a contour plot of CO mass fraction for the W2 simulation is shown in Fig. 3.6. An exponential distribution of contour levels is used to emphasize the extent of the incomplete combustion at the choke of the burner. When the plots of temperature, O2, and CO are considered together, it is apparent that the simulation predicts a highly swirling diffusion ame at the choke with cool air surrounding hot, partially burned gases. Density stratification impedes the mixing of the fuel and oxidant. Mixing (and the resultant oxidation of CO) downstream of the choke should cause the high levels of CO (of about 5000 ppm) to significantly decrease.

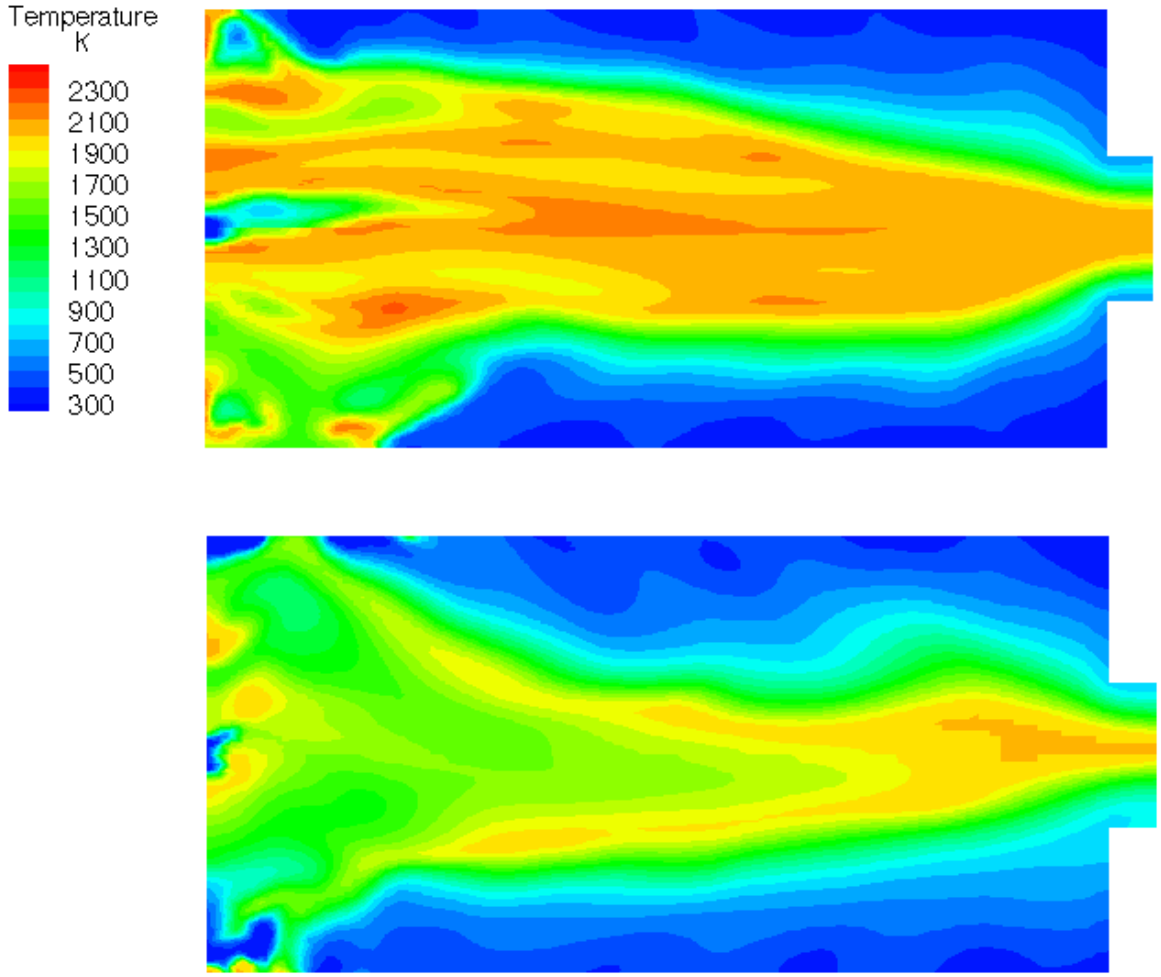

Figure 3.3: Static temperature (K) on the vertical, centerline plane with fuel entering from the top. The top panel is from simulation M3 and the bottom is from simulation W2.

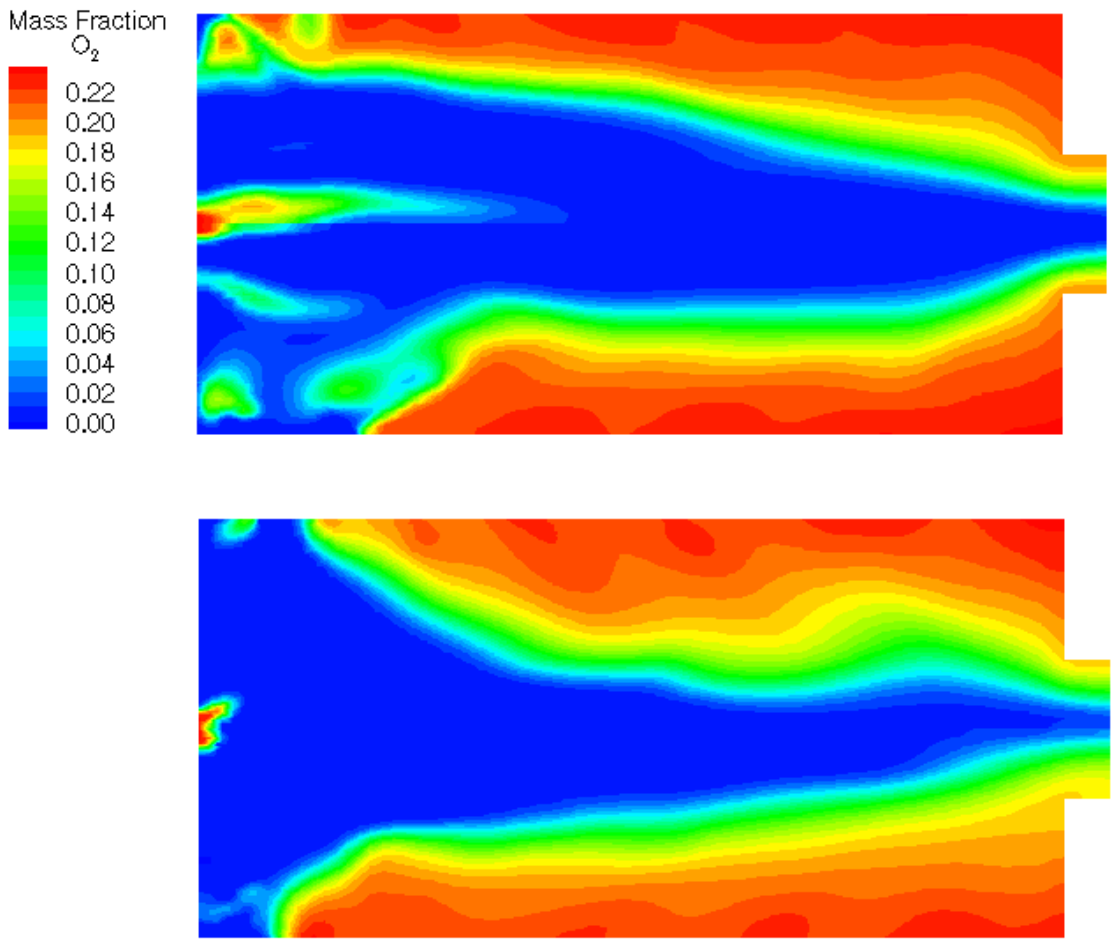

Figure 3.4: Mass fraction of O_2 on the vertical, centerline plane with fuel entering from the top. The top panel is from simulation M3 and the bottom is from simulation W2.

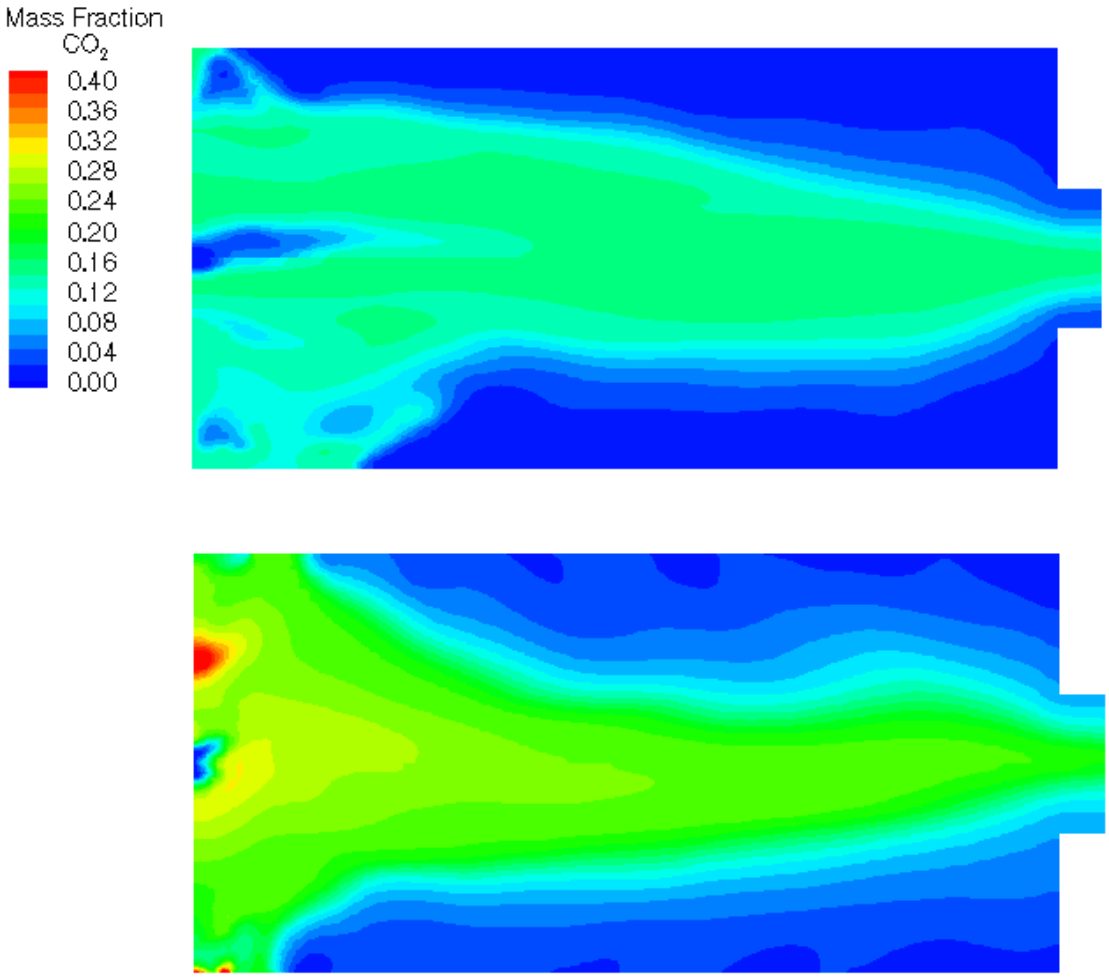

Figure 3.5: Mass fraction of CO_2 on the vertical, centerline plane. The top panel is from simulation M3 and the bottom is from simulation W2.

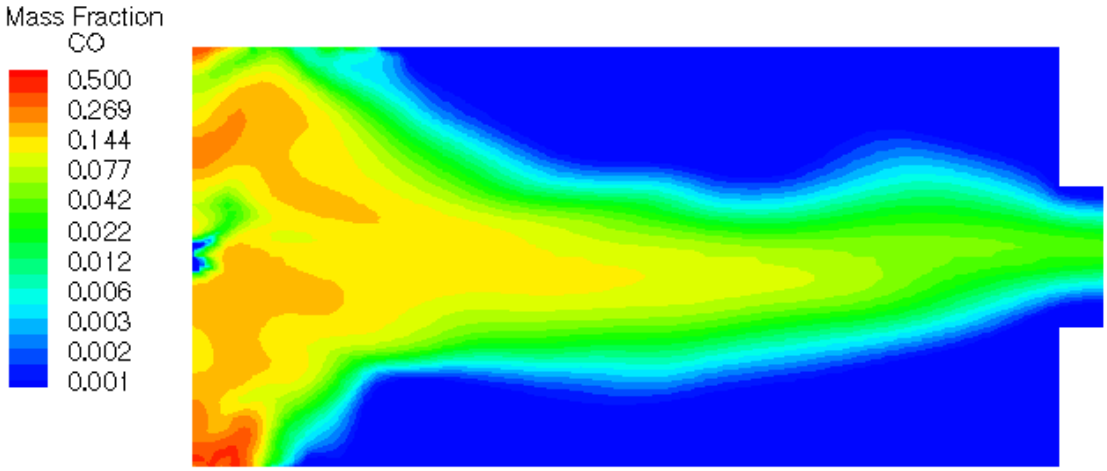

Figure 3.6: Mass fraction of CO on the vertical, centerline plane for simulation W2.

Chapter 4

NO_X Production

In Chapter 3, it is shown that the temperatures and major species concentrations in simulation W2 are consistent with expected values and, therefore, that this simulation can be used as the basis for predicting thermal and fuel NO_x production in the McConnell burner. In the current chapter, the W2 results were post-processed to predict NO_x and HCN concentrations with various scenarios. The overall results are shown in Table 4 below. The scenarios listed in the table span ranges of fuel nitrogen content, volatile nitrogen content, and char BET surface area, with the first row in the table representing reasonable estimates for wood dust and the last row representing estimates for a wood dust containing a large amount of urea formaldehyde resin (Malte et al., 1996). The volatile nitrogen is assumed to undergo devolatilization at the same rate as the carbon. The balance of the nitrogen, i.e., the char nitrogen, undergoes conversion by heterogenous reaction. In the column of Table 4 labeled "Max. Fuel NO_x" are shown the fuel NO_x concentrations that would occur if all the fuel nitrogen were converted to NO_x. In Figs. 4.1-4.5 are shown the NO and HCN concentrations on the vertical cut through the centerline for each scenario; these figures are discussed below.

The fuel nitrogen concentrations are computed assuming that the char nitrogen is converted to NO rather than to HCN, which is consistent with the earlier assumption that the carbon in the char oxidizes to CO_2 via (2.3a). When 93% of the fuel nitrogen devolatilizes, the conversion path that the remaining 7% of the nitrogen takes has little impact on the total amount of NO_x produced. The value of 93% volatile nitrogen is selected to match the overall volatile yield of the wood dust used in the modeling. However, to examine the impact of retention of nitrogen in the char, 50% volatile nitrogen is also treated in the modeling.

The effect of thermal NO_x on the total NO_x emissions is shown in the table for each scenario.

Table 4.1: NO_x mass fractions (Y_i) and concentrations at the exit plane of simulation W2. Mass fractions are $\times 10^6$. Concentrations are in parts per million dry basis adjusted to 18% O_2.

Scenario	Mass % N in fuel	% of N devol.	A_{BET} (m^2/kg)	Thermal NO_x		Fuel NO_x		Thermal + Fuel NO_x			Max. Fuel NO_x	Y_{HCN}
				Y_{NO_x}	ppmvd	Y_{NO_x}	ppmvd	Y_{NO_x}	ppmvd	#/MMBtu[a]	ppmvd	
W2-1	0.10	0.93	25000	19.5	7.5	50.8	20	69	26.5	0.18	51	0.094
W2-2	2.83	0.93	25000	19.5	7.5			373	145	0.97	1332	6.4
W2-3	5.65	0.50	0	19.5	7.5			1088	421	2.82	2700	0.24
W2-4	5.65	0.50	25000	19.5	7.5	845	327	857	332	2.22	2700	2.7
W2-5	5.65	0.93	25000	19.5	7.5	570	221	581	226	1.51	2700	13

[a] NO_x assigned the molecular weight of NO_2

When only the model for thermal NO_x is enabled, the NO_x concentration at the exit plane is 7.5 parts per million on a dry volume basis adjusted to 18% O_2 (ppmvd). Adjustment to 18% O_2 is used since this is the nominal O_2 content found in the stack gas of dryers heated by dust-fired burners. In the case of pure wood dust (0.1% nitrogen in the fuel), 7.5 ppmvd is a significant portion of the total NO_x emission. For the cases with higher fuel nitrogen contents, the thermal NO_x is insignificant. Also, the thermal and fuel NO_x interact, so that the sum of the concentrations computed when each mechanism is run separately are greater than the concentration predicted when the mechanisms are run together.

We begin our analysis of fuel NO_x production with scenario W2-1 (Fig. 4.1). In this scenario, 93% of the fuel nitrogen is released from the wood particles in the volatiles so that the primary path for production of NO is via HCN. The concentration of NO is shown in the top panel of the figure and the concentration of HCN in the bottom panel. The HCN is produced very soon after the volatiles are released from the particles as evidenced by the high concentration of HCN in the inlet end of the burner away from the burner centerline. The HCN rapidly oxidizes to NO resulting in the highest concentrations of NO in the upstream end of the burner. In the downstream section of the burner, the competition between various fuel species for oxygen is strong in the diffusion flame that is established with fuel species in the core of the burner surrounded by oxidant. At the same time, the core region is hot enough (Fig. 3.3) to support the mutual destruction of HCN and NO via the reduction reaction with the rate given by (2.29). Consequently, competition between oxidation of HCN to NO and reduction of NO by HCN to N_2 occurs, with the overall behavior being a decrease in NO as the flow progresses downstream in the burner. The conversion of fuel nitrogen to NO for this scenario is very high (52%).

The HCN is an intermediate of the fuel-nitrogen conversion process, and in the simulations, it is the only fixed nitrogen species that links the fuel-nitrogen to the final products (NO and N_2). This simplification of the fuel-nitrogen conversion process results from basing the current model mechanism on those presented in the literature on coal combustion. However, in wood flames, as well as in flames for some ranks of coal, ammonia (NH_3) also serves as a fixed-nitrogen intermediate. Thus, in interpreting the present simulations, it may be best to regard HCN as a general fixed-nitrogen intermediate. Although HCN surely exists in the flames of wood burners, its concentration is probably less than indicated in the current simulations and NH_3 is probably also present. The lack of oxygen in the core of the combustor in the simulations also promotes the large concentrations

of HCN observed. The long, hot core and the surrounding diffusion flame are dominant features of the present simulations and are consistent with a lack of O_2 and an abundance of intermediate fixed-nitrogen in the core.

In scenario W2-2 (Fig. 4.2), more nitrogen is added to the fuel to represent a dust of wood containing resin; all other parameters are the same as in scenario W2-1. The formation and destruction of NO is generally similar to that in the case of pure wood dust, but now, because of the larger amount of fuel nitrogen, the HCN concentration in the core is very large, leading to consumption of the O_2 that penetrates there and reduction of NO to N_2. The diffusion flame surrounding the core flow is more pronounced. Consequently, the conversion of fuel nitrogen to NO_x in this scenario is only 11%.

In scenarios W2-3, W2-4, and W2-5 the fuel nitrogen is increased to the level observed in the wood-with-resin dust analyzed by Malte et al. (1996). This is a "high-resin" fuel. In these simulations, volatile nitrogen and the BET surface area (A_{BET}) are varied in order to observe the effect of the several situations for production and destruction of NO. In scenario W2-3 (Fig. 4.3), the volatile nitrogen is reduced to 50%, and $A_{\mathrm{BET}} = 0$, which disables the reduction of NO on the char surface. In the top panel of the figure, the concentration of NO in the core region is very high. The surface reduction mechanism is unavailable to play an important role in the destruction of NO in this region. Also, less HCN is available to reduce NO to N_2.

In scenario W2-4 (Fig. 4.4), all parameters are the same as in W2-3 except the surface reduction mechanism is enabled. The result is a substantial reduction in the NO concentration and an increase in the HCN concentration at the exit plane. In scenario W2-5, it is assumed that the nitrogen in the volatiles is proportional to the fraction of fuel mass that devolatilizes, i.e., 93%. This assumption increases the amount of HCN that is formed and decreases the amount of NO formed directly. However, due to the competition between the HCN oxidation and reduction reactions, a six-fold decrease in the amount of NO formed directly results in a 32% decrease in NO at the exit plane. The conversion rate for fuel nitrogen in scenario W2-5 is 8.4%, which is the lowest conversion of fuel-nitrogen to NO observed in the simulations with high-resin fuel.

The preferred method of reporting NO_x emissions for industrial burners is as pounds of NO_x (as NO_2) per fuel input as millions of Btu on a HHV basis (MMBtu). The emissions are shown in these units in Table 4. For the simulations of the wood dust without resin, the result is 0.18 #/MMBtu, which is in the range expected for a wood dust burner. For the simulation of high-resin wood

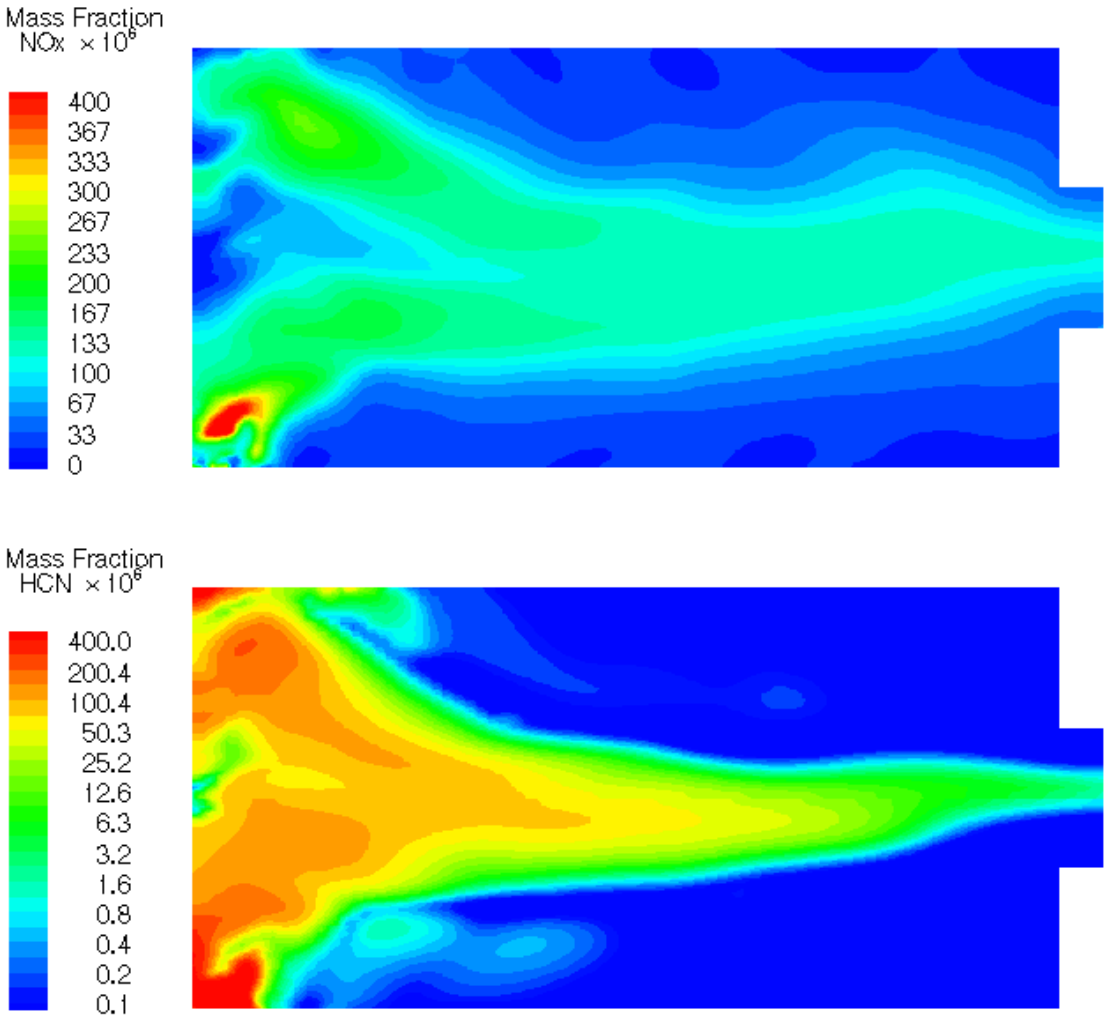

Figure 4.1: Mass fraction of NO and HCN on the vertical, centerline plane for simulation W2-1.

dust (W2-5), the result is 1.51 #/MMBtu. Field burner data to which we have access indicates an emission of 1.3 to 1.4 #/MMBtu for a high-resin wood dust burned without supplemental gas firing. Thus, the simulations appear to be providing a useful picture of the fuel-nitrogen conversion in the dust burner.

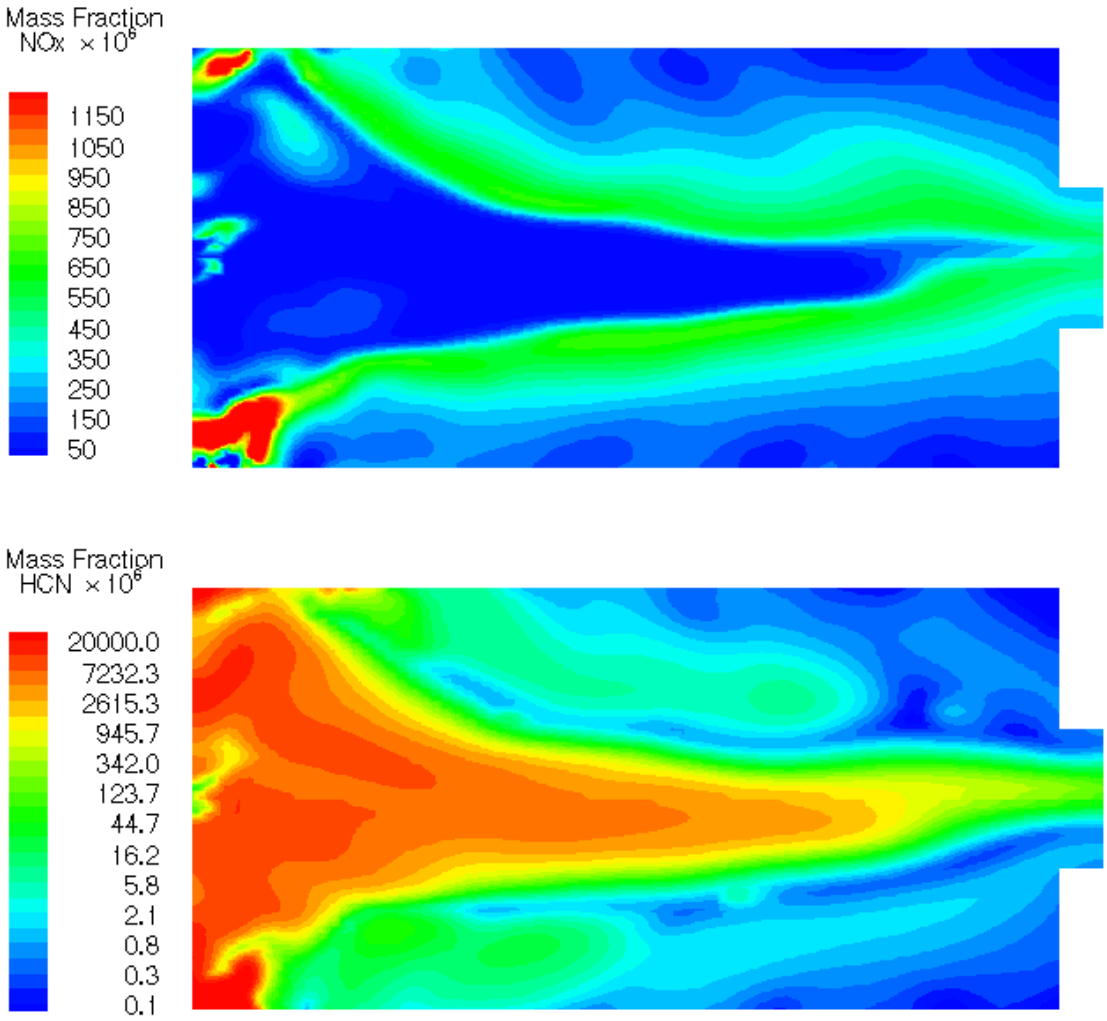

Figure 4.2: Mass fraction of NO and HCN on the vertical, centerline plane for simulation W2-2.

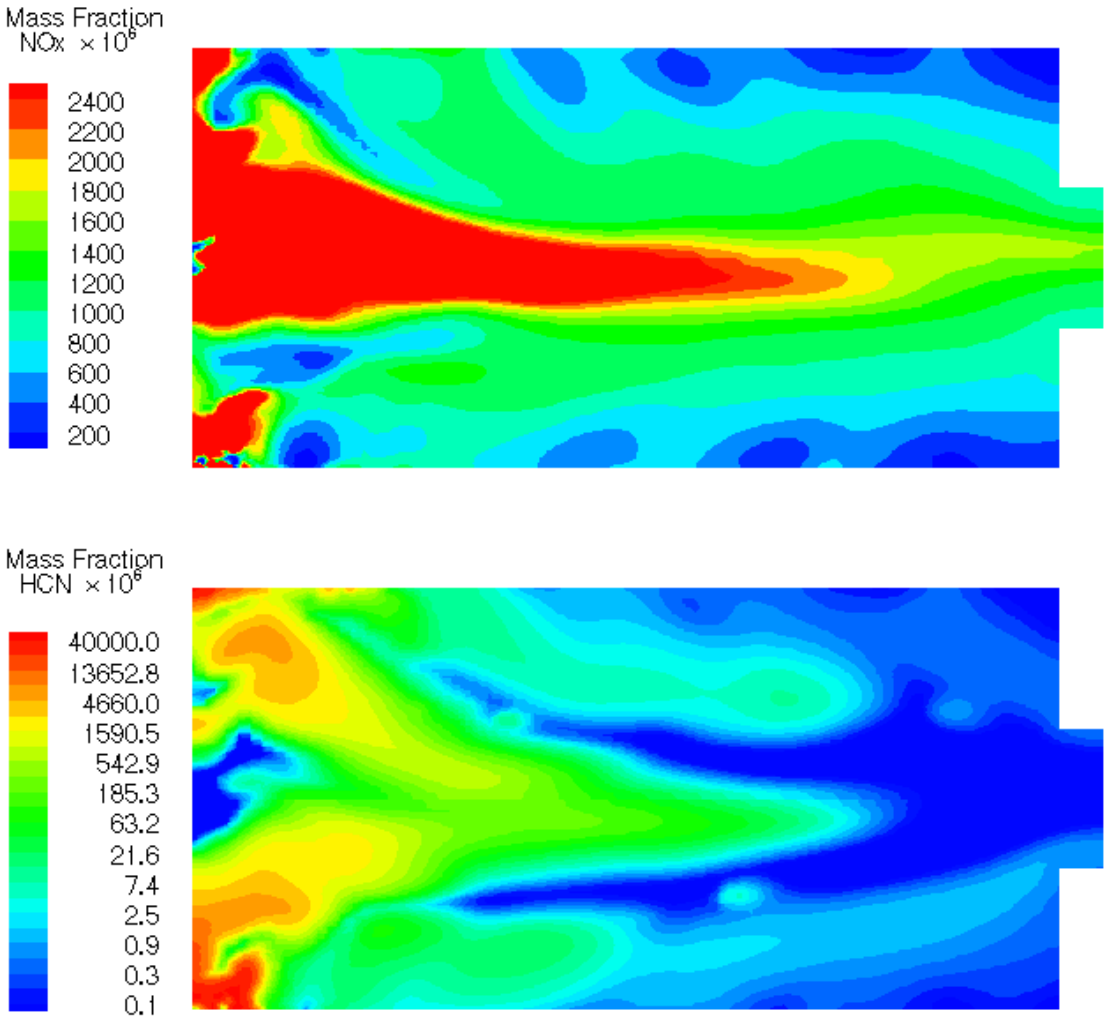

Figure 4.3: Mass fraction of NO and HCN on the vertical, centerline plane for simulation W2-3.

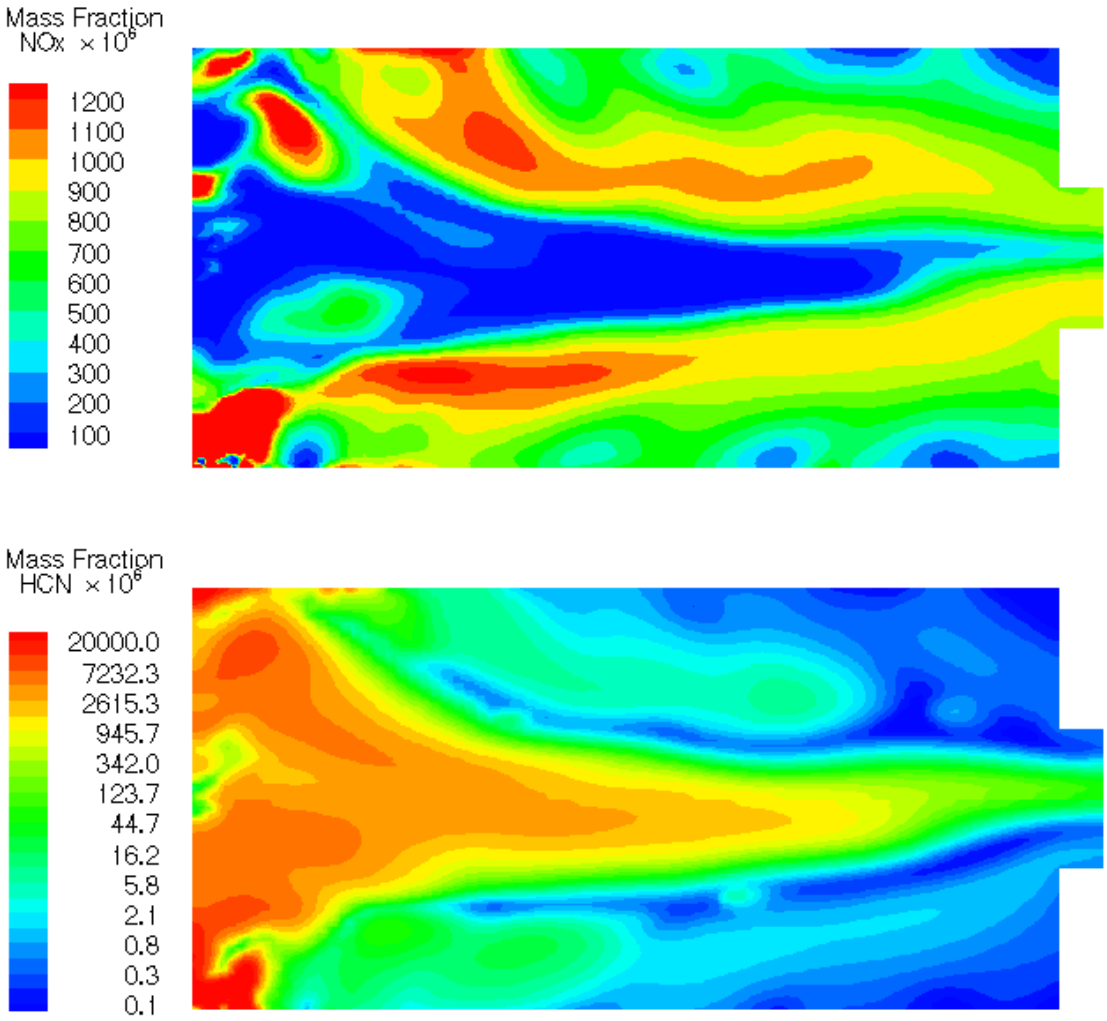

Figure 4.4: Mass fraction of NO and HCN on the vertical, centerline plane for simulation W2-4.

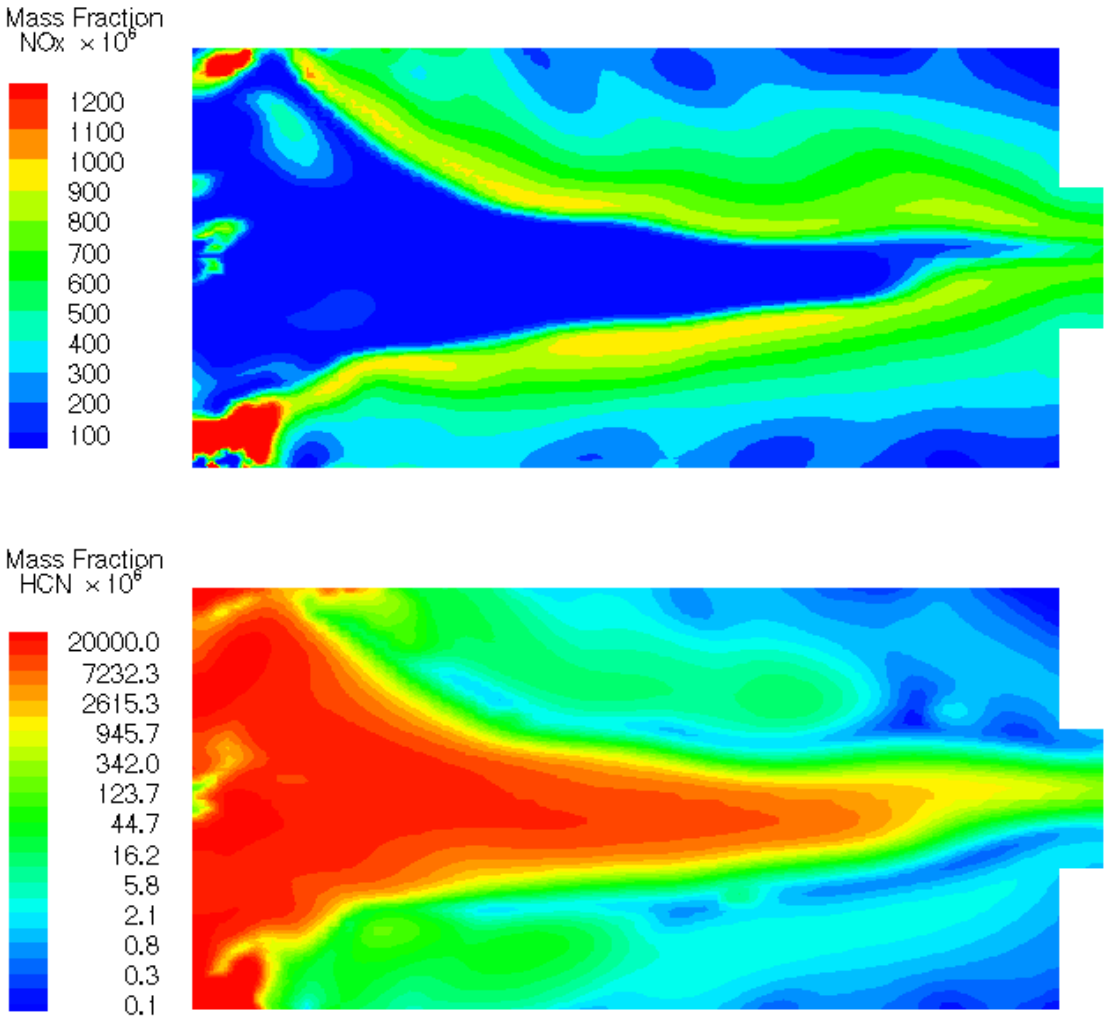

Figure 4.5: Mass fraction of NO and HCN on the vertical, centerline plane for simulation W2-5.

Chapter 5

Conclusions

The focus of this research has been on the modeling and the prediction of NO_x concentrations in the cyclone wood dust burner. The FLUENT NO_x model requires, among other parameters, inputs for the fraction of fuel nitrogen that devolatalizes and the BET surface area of the char, and neither of these quantities is well known for wood dust. Decreasing the BET surface area has the same effect as decreasing the volatile nitrogen fraction, i.e., it increases the exit plane NO_x concentration. Fortunately, the concentration of NO_x at the exit plane increases by only a factor of 1.9 when the BET surface area is reduced from 25000 to 0 (m^2=kg) and the volatile nitrogen fraction is reduced from 93% to 50%. The conclusion is that modest uncertainty in either of the input parameters will not lead to significant errors in the NO_x predictions. This encourages the thought that the development of the current simulations can lead to insight into how to reduce NO_x emissions from wood dust burners.

Observation of the exit plane concentrations of CO and HCN indicate that the chemical reactions are not complete by the time the gases pass through the choke of the burner. Completion of reaction will occur downstream of the choke of the main cyclonic combustion chamber modeled in this report.

Other Research on Modeling Wood Burners

Other research conducted by the University of Washington Energy and Environmental Combustion Laboratory on the modeling of wood dust burners includes the following:

1. CFD modeling of a laboratory dust burner. This work will help to verify the modeling approach and the chemical rates, through the comparison of the modeling results to an existing data base for the laboratory burner.

2. CRN modeling of the laboratory and industrial wood dust burner. CRN stands for Chemical Reactor Network. CRNs allow a much fuller chemistry to be applied to the problem, and generally permit faster computations. Thus, they can in general be used more easily by the design engineer than CFD.

These other researches are scheduled to be completed in 2005.

Other Research on Modeling Burners

Other research conducted by the University of Washington Energy and Environmental Combustion Laboratory on the modeling of burners is focused on the following:

1 Development of global chemical kinetic mechanisms.

2 CFD and CRN modeling of lean premixed combustors, especially as used in low emission power generation gas turbines

Acknowledgments

This research is supported by the U.S. Department of Energy (grant no. DE-FC07-001D13869). Computing resources were provided by Intel Corporation and by the National Science Foundation (grant no. DMI9617754). The authors thank Dr. Mark Ganter for assistance with the "Beowulf cluster" used for the simulations.

Bibliography

Aho, M. J., J. P. Hämäläinen, and J. L. Tummavuori (1993). Importance of solid-fuel properties to nitrogen-oxide formation through HCN and NH_3 in small-particle combustion. *Combust. Flame 95*(1-2), 22–30.

Anthony, D. B. and J. B. Howard (1975). Coal devolatilization and hydrogasification. *AIChE J. 22*, 625.

Badzioch, S. and P. G. W. Hawksley (1970). Kinetics of thermal decomposition of pulverized coal particles. *Ind. Eng. Chem. Process Des. Dev. 9*, 521.

Baum, M. M. and P. J. Street (1971). Predicting the combustion behavior of coal particles. *Combust. Sci. Technol. 3*(5), 231–243.

Bilger, R. W. and R. E. Beck (1975). In *15th Symp. (Int'l.) on Combustion*, pp. 541. The Combustion Institute.

Blauwens, J., B. Smets, and J. Peeters (1977). Mechanism of "prompt" NO formation in hydrocarbon flames. In *16th Symp. (Int'l.) on Combustion*, pp. 1055–1064. The Combustion Institute.

Boussinesq, J. (1877). Théorie de l'écoulement tourbillant. *Mem. Présentés par Divers Savants Acad. Sci. Inst. Fr. 23*, 46–50.

Boyd, R. K. and J. H. Kent (1986). Three-dimensional furnace computer modeling. In *21st Symp. (Int'l) on Combustion*, pp. 265–274. The Combustion Institute.

Boysan, F., R. Weber, J. Swithenbank, and C. J. Lawn (1986). Modeling coal-fired cyclone combustors. *Combust. Flame 63*(1-2), 73–86.

Brunauer, S. (1943). *The Absorption of Gases and Vapors.* Princeton, NJ: Princeton University Press.

Chen, J. C. and C. A. Lin (1999). Computations of strongly swirling flows with second-moment closures. *Int. J. Numer. Meth. Fl. 30*(5), 493–508.

de Soete, G. G. (1975). Overall Reaction Rates of NO and N_2 Formation from Fuel Nitrogen. In *15th Symp. (Int'l.) on Combustion*, pp. 1093. The Combustion Institute.

Field, M. A. (1969). Rate of combustion of size-graded fractions of char from a low rank coal between 1200 K–2000 K. *Combust. Flame 13*, 237–252.

Flower, W. L., R. K. Hanson, and C. H. Kruger (1975). In *15th Symp. (Int'l.) on Combustion*, pp. 823. The Combustion Institute.

Hanson, R. K. and S. Salimian (1984). Survey of Rate Constants in H/N/O Systems. In W. C. Gardiner (Ed.), *Combustion Chemistry*, pp. 361.

Hogg, S. and M. A. Leschziner (1989a). 2nd-moment-closure calculation of strongly swirling confined flow with large density gradients. *Int. J. Heat Fluid Fl. 10*(1), 16–27.

Hogg, S. and M. A. Leschziner (1989b). Computation of highly swirling confined flow with a Reynolds stress turbulence model. *AIAA J. 27*(1), 57–63.

Kobayashi, H., J. B. Howard, and A. F. Sarofim (1976). Coal devolatilization at high temperatures. In *16th Symp. (Int'l) on Combustion*. The Combustion Institute.

Launder, B. E. and D. B. Spalding (1974). The numerical computation of turbulent flows. *Computer Methods in Applied Mechanics and Engineering 3*, 269–289.

Leppälahti, J. and T. Koljonen (1995). Nitrogen evolution from coal, peat and wood during gasification – literature-review. *Fuel Processing Technology 43*(1), 1–45.

Levy, J. M., L. K. Chen, A. F. Sarofim, and J. M. Beer (1981). NO/Char Reactions at Pulverized Coal Flame Conditions. In *18th Symp. (Int'l.) on Combustion*. The Combustion Institute.

Lockwood, F. C. and C. A. Romo-Millanes (1992, September). Mathematical Modelling of Fuel - NO Emissions From PF Burners. *J. Int. Energy 65*, 144–152.

Magnussen, B. F. and B. H. Hjertager (1976). On mathematical models of turbulent combustion with special emphasis on soot formation and combustion. In *16th Symp. (Int'l.) on Combustion*. The Combustion Institute.

Malte, P. C. and D. G. Nicol (1997). Engineering analysis of NOx formation in wood dust burners: Application to the Marshfield plant. Technical report, Department of Mechanical Engineering, University of Washington.

Malte, P. C., D. G. Nicol, and T. Rutar (1996). Development of a model for predicting the NOx emissions of burners fired with sawdusts and sanderdusts high in nitrogen. Technical report, Department of Mechanical Engineering, University of Washington.

Monat, J. P., R. K. Hanson, and C. H. Kruger (1979). In *17th Symp. (Int'l.) on Combustion*, pp. 543. The Combustion Institute.

Nunn, T. R., J. B. Howard, J. Longwell, and W. A. Peters (1985). Product compositions and kinetics in the rapid pyrolysis of sweet gum hardwood. *Ind. Eng. Chem. Process Des. Dev. 24*(3), 836–844.

Pope, S. (1985). Pdf methods for turbulent reactive flows. *Progress in Energy and Combustion Science 11*, 119–192.

Smith, I. W. (1982). The combustion rates of coal chars: A review. In *19th Symp. (Int'l) on Combustion*, pp. 1045–1065. The Combustion Institute.

Smoot, L. D. and P. J. Smith (1985). *Coal Combustion and Gasification*. New York: Plenum Press.

Tillman, D. A. (1991). *The Combustion of Solid Fuels And Wastes*. San Diego: Academic Press.

Turns, S. R. (2000). *An Introduction to Combustion. Concepts and Applications* (2 ed.). McGraw-Hill.

Westbrook, C. K. and F. L. Dryer (1984). Chemical kinetic modeling of hydrocarbon combustion. *Prog. in Energy and Combust. Sci. 10*, 1–57.

Wilcox, D. C. (1993). *Turbulence Modeling for CFD*. La Canada, California: DCW Industries, Inc.

Williams, F. A. (1975). *Turbulent Mixing in Nonreactive and Reactive Flows*. New York: Plenum Press.

Zhang, J. and S. Nieh (1997). Comprehensive modelling of pulverized coal combustion in a vortex combustor. *Fuel 76*(2), 123–131.